Emergent Model for Predicting the Average Surface Temperature of Rocky Planets with Diverse Atmospheres

Den Volokin, Ph.D.
E-mail: dvolokin@gmail.com

Lark ReLlez, Ph.D.
Tso Consulting, 843 E Three Fountains Suite 260, Salt Lake City, UT 84107 U.S.A.

Published: *Advances in Space Research*, Aug. 18 2015, doi: 10.1016/j.asr.2015.08.006

Abstract

The Global Mean Annual near-surface Temperature (GMAT) of a planetary body is an expression of the available kinetic energy in the climate system and a critical parameter determining planet's habitability. Previous studies have relied on theory-based mechanistic models to estimate GMATs of distant bodies such as extrasolar planets. This 'bottom-up' approach oftentimes utilizes case-specific parameterizations of key physical processes (such as vertical convection and cloud formation) requiring detailed measurements in order to successfully simulate surface thermal conditions across diverse atmospheric and radiative environments. Here, we present a different 'top-down' statistical approach towards the development of a universal GMAT model that does not require planet-specific empirical adjustments. Our method is based on Dimensional Analysis (DA) of observed data from the Solar System. DA provides an objective technique for constructing relevant state and forcing variables while ensuring dimensional homogeneity of the final model. Although widely utilized in other areas of physical science to derive models from empirical data, DA is a rarely employed analytic tool in astronomy and planetary science. We apply the DA methodology to a well-constrained data set of six celestial bodies representing highly diverse physical environments in the solar system, i.e. Venus, Earth, the Moon, Mars, Titan (a moon of Saturn), and Triton (a moon of Neptune). Twelve prospective relationships (models) suggested by DA are investigated via non-linear regression analyses involving dimensionless products comprised of solar irradiance, greenhouse-gas partial pressure/density and total atmospheric pressure/density as forcing variables, and two temperature ratios as dependent (state) variables. One non-linear regression model is found to statistically outperform the rest by a wide margin. Our analysis revealed that GMATs of rocky planets can accurately be predicted over a broad range of atmospheric conditions and radiative regimes only using two forcing variables: top-of-the-atmosphere solar irradiance and total surface atmospheric pressure. The new model displays characteristics of an emergent macro-level thermodynamic relationship heretofore unbeknown to science that deserves further investigation and possibly a theoretical interpretation.

Keywords: dimensional analysis; emergent model; planetary temperature; atmospheric thermal enhancement; greenhouse gas; atmospheric pressure

1. Introduction

The Global Mean Annual near-surface Temperature (GMAT) of a celestial body is a physical manifestation of the available kinetic energy in the climate system. This energy determines the type of solvent that could exist on the surface and controls, along with atmospheric composition and density, a number of important geophysical and geochemical processes such as erosion, rock weathering and sedimentation. GMAT is also a critical parameter determining a planet's habitability (Kaltenegger and Sasselov 2011; Schulze-Makuch et al. 2011; Leconte et al. 2013). Thus, frigid temperatures of around -179 C and 1.467 bar of atmospheric pressure on the surface of Saturn's moon Titan enable the existence of large hydrocarbon lakes as well as methane/ethane relative humidity in the air and methane precipitation (Hayes et al. 2008; Raulin 2008; Griffith 2009; Sharma and Byrne 2011). Although water is likely abundant on the surface of Titan (Iess et al. 2012), it plays insignificant role in that moon's surface geochemistry, since it occurs in a rock-hard form that cannot sublimate due to a high atmospheric pressure and an extremely cold environment (NASA Solar System Exploration 2014). At the same time, balmy temperatures of about +14 C and nearly 1 bar of air pressure on Earth allow water rather than methane to cycle between surface and the atmosphere forming liquid oceans that cover almost 71% of our planet. Because of the warm environment on Earth, methane cannot exist in a liquid form at the surface and only occurs as a minor trace gas in the atmosphere. Interestingly, however, the methane cycle on Titan plays a very similar geophysical role to the hydrological cycle on Earth. Nevertheless, a stark contrast exists in the physical environment, regolith composition, and surface geochemistry between Titan and Earth that is largely explainable by the vastly different thermal conditions found on the two bodies.

Thus, having a general model available that can accurately predict GMATs of rocky planets as a function of a few remotely measurable parameters would be highly beneficial to both planetary science and astrobiological research. Current process-oriented climate models built on theoretical concepts utilize planet-specific parameterizations of key processes such as vertical convection and cloud nucleation in order to successfully simulate planetary thermal environments across a wide range of illumination and atmospheric conditions (Bengtsson et al. 2013, Chapter 1). Such empirical parameterizations oftentimes require detailed measurements that are not always available. The impetus of this study was to explore the feasibility for deriving a simple yet robust planetary temperature model of high predictive skill that uses a common set of drivers while requiring no case-specific empirical adjustments of model parameters. Our goal was based on the premise that the same general processes controlling Earth's global temperature are also responsible for creating the observed pattern of planetary temperatures across the Solar System.

Unlike past studies which employed reductionist methods rooted in theory, we adopt a 'top-down' empirical approach based on Dimensional Analysis (DA) of observed data from the Solar System. DA was chosen as an analytic tool in our model development because of

its ubiquitous past successes in solving complex problems of physics, engineering, mathematical biology, and biophysics (e.g. Rashevsky 1960; Albertson et. al. 1961; Yalin 1971; Taylor 1974; Bender 1978; Vignaux and Jain 1988). To our knowledge, DA has not previously been applied to constructing predictive models of macro-level properties such as the average global temperature of a planet; thus, an overview of this technique could help better understand our analysis.

1.1. Dimensional Analysis background

DA is a method for extracting physically meaningful relationships from empirical data (Huntley 1967; Vignaux 1991; Vignaux and Scott 1999). The goal of DA is to restructure a set of original variables deemed critical to describing a physical phenomenon into a smaller set of independent *dimensionless* products that may be combined into a dimensionally homogeneous model of predictive power. Dimensional homogeneity is a prerequisite for any robust physical relationship such as natural laws. It means that all terms of a model equation subjected to addition, subtraction, or rising to powers have the same dimensions; in this case, they would be dimensionless. DA distinguishes between *measurement units* and *physical dimensions*. For example, *mass* is a physical dimension that can be measured in gram, pound, metric ton etc.; *time* is another dimension measurable in seconds, hours, years etc. While the physical dimension of a variable is always the same, the units quantifying that variable may vary depending on the adopted measurement system. DA is mainly concerned with physical dimensions rather than measurement units.

Many physical variables and constants can be described in terms of four fundamental dimensions, i.e. *mass* [M], *length* [L], *time* [T], and *absolute temperature* [Θ]. For example, an energy flux commonly measured in W m^{-2} has a physical dimension [M T^{-3}] since 1 W m^{-2} = 1 J s^{-1} m^{-2} = 1 (kg m^2 s^{-2}) s^{-1} m^{-2} = kg s^{-3}. Pressure may be reported in units of Pascal, bar, atm., PSI, or Torr, but its physical dimension is always [M L^{-1} T^{-2}] because 1 Pa = 1 N m^{-2} = 1 (kg m s^{-2}) m^{-2} = 1 kg m^{-1} s^{-2}. Thinking in terms of dimensions rather than measurement units fosters a deeper understanding of the underlying physical relationships. For instance, a comparison between the physical dimensions of energy flux and pressure reveals that a flux is simply the product of pressure and the speed of moving particles [L T^{-1}], i.e. [M T^{-3}] = [M L^{-1} T^{-2}] [L T^{-1}]. Therefore, a radiative flux F_R (W m^{-2}) can be expressed in terms of photon pressure p_ν (Pa) and the speed of light c (m s^{-1}) as $F_R = p_\nu\, c$. Since c is constant within a medium, varying the intensity of electromagnetic radiation in a given medium effectively means altering the pressure of photons. Indeed, the solar radiation reaching Earth's upper atmosphere exerts a pressure (force) of sufficient magnitude to perturb the orbits of communication satellites over time (e.g. van der Ha and Lappas 2007; McMahon and Scheeres 2010).

The simplifying power of DA in model development stems from the Buckingham Pi Theorem (Buckingham 1914), which states that a problem involving n *dimensioned* x_i variables, i.e.

$$f(x_1, x_2, \dots, x_n) = 0$$

can be reformulated into a less complicated relationship of $(n - m)$ *dimensionless* π_i products derived from x_i, i.e.

$$\phi(\pi_1, \pi_2, \dots, \pi_{n-m}) = 0$$

where m is the number of fundamental dimensions comprising the original variables. This theorem determines the number of non-dimensional π_i variables to be found in a set of products, but it does not prescribe the number of sets that could be generated from the original variables defining a particular problem. In other words, there might be, and oftentimes is more than one set of $(n - m)$ dimensionless products to analyze. DA provides an objective method for constructing the sets of π_i variables employing simultaneous equations solved via either matrix inversion or substitution (e.g. Huntley 1967).

The second step in DA (following the construction of dimensionless products) is to search for a functional relationship between the π_i variables of each set using regression analysis. DA does not disclose the best function capable of describing an empirical dataset. It is the investigator's responsibility to identify a suitable regression model based on prior knowledge of the phenomenon and a general expertise in the subject area. DA only guarantees that the final model (whatever its functional form) will be dimensionally homogeneous, hence it may qualify as a physically meaningful relationship provided that it (*a*) is not based on a simple polynomial fit; (*b*) has a small standard error; (*c*) displays high predictive skill over a wide range of input data; and (*d*) is statistically robust. The regression coefficients of the final model will also be dimensionless, and may reveal true constants of Nature by virtue of being independent of the units utilized to measure the driving variables.

2. Methods

A planet's GMAT depends on many factors. In our study, we focused on drivers that are remotely measurable and/or theoretically estimable. Based on the current state of knowledge we identified seven physical variables of potential relevance to the surface temperature: (1) top-of-the-atmosphere (TOA) stellar irradiance (S); (2) mean planetary surface temperature in the absence of atmospheric greenhouse effect, hereto called reference temperature (T_r); (3) near-surface partial pressure of atmospheric greenhouse gases (P_{gh}); (4) near-surface mass density of atmospheric greenhouse gases (ρ_{gh}); (5) total surface atmospheric pressure (P); (6) total surface atmospheric density (ρ); and (7) minimum air pressure required for the existence of a liquid solvent at the surface, hereto called reference pressure (P_r). Table 1 lists

Table 1 Variables employed in the Dimensional Analysis aimed at deriving a general planetary temperature model. The variables are comprised of 4 fundamental physical dimensions: *mass* [M], *length* [L], *time* [T] and *absolute temperature* [Θ].

Planetary Variable	Symbol	SI Units	Physical Dimension
Global mean annual near-surface temperature (GMAT), the dependent variable	T_s	K	[Θ]
Stellar irradiance (average shortwave flux incident on a plane perpendicular to the stellar rays at the top of a planet's atmosphere)	S	W m^{-2}	[M T^{-3}]
Reference temperature (planet's mean surface temperature in the absence of atmospheric greenhouse effect)	T_r	K	[Θ]
Average near-surface gas pressure representing either partial pressure of greenhouse gases or total atmospheric pressure	P_x	Pa	[M L^{-1} T^{-2}]
Average near-surface gas density representing either greenhouse-gas density or total atmospheric density	ρ_x	kg m^{-3}	[M L^{-3}]
Reference pressure (i.e. minimum atmospheric pressure required for the presence of a liquid solvent at the surface)	P_r	Pa	[M L^{-1} T^{-2}]

the above variables along with their SI units and physical dimensions. Note that, in order to simplify the derivation of dimensionless products, pressure and density are represented in Table 1 by the generic variables P_x and ρ_x, respectively. As explained below, the regression analysis that follows the construction of π_i variables explicitly distinguishes between models involving partial pressure/density of greenhouse gases and those employing total atmospheric pressure/density at the surface. The planetary Bond albedo (α_p) was intentionally not selected as an explicit temperature driver in our DA despite its known effect on the surface energy budget, because it is already dimensionless and partakes in the computation of reference temperatures discussed in Section 2.1.

Appendix A details the procedure employed to construct the π_i variables. DA yielded two sets of π_i products, each one consisting of two dimensionless variables, i.e.

$$\pi_1 = \frac{T_s}{T_r}; \qquad \pi_2 = \frac{P_x^3}{\rho_x S^2} \qquad | \quad \text{Set 1}$$

and

$$\pi_1 = \frac{T_s}{T_r}; \qquad \pi_2 = \frac{P_x}{P_r} \qquad | \quad \text{Set 2}$$

This implies an investigation of two basic types of dimensionally homogeneous functions (relationships):

$$\frac{T_s}{T_r} = f\left(\frac{P_x^3}{\rho_x S^2}\right) \qquad (1)$$

and

$$\frac{T_s}{T_r} = f\left(\frac{P_x}{P_r}\right) \qquad (2)$$

Note that $\pi_1 = T_s/T_r$ occurs as a dependent variable in both functions, since it contains the sought temperature T_s. Upon replacing the generic pressure/density variables P_x and ρ_x in Eqs. (1) and (2) with either partial pressure/density of greenhouse gases (P_{gh} and ρ_{gh}) or total atmospheric pressure/density (P and ρ), one arrives at six prospective regression models. Further, as discussed in Section 2.1, we employ two distinct kinds of reference temperature calculated from different formulas, i.e. an effective radiating equilibrium temperature (T_{e}) and a mean '*no-atmosphere*' spherical surface temperature (T_{na}). This doubles the π_1 instances in the regression analysis bringing the total number of potential models for investigation to 12.

2.1. Reference Temperatures and Reference Pressure

A reference temperature (T_r) characterizes the average thermal environment of a planetary body in the absence of atmospheric greenhouse effect; hence, T_r is different for each body depending on its solar irradiance and albedo. The purpose of T_r is to provide a baseline for quantifying the thermal effect of planetary atmospheres. Indeed, the T_s/T_r ratio produced by DA can physically be interpreted as a Relative Atmospheric Thermal Enhancement (RATE) ideally expected to be equal to or greater than 1.0. Expressing the thermal effect of a planetary atmosphere as a non-dimensional quantity rather than an absolute temperature difference (as done in the past) allows for an unbiased comparison of the greenhouse effects of celestial bodies orbiting at different distances from the Sun. This is because the absolute strength of the greenhouse effect (measured in K) depends on both solar insolation and atmospheric properties, while RATE is only expected to be a function of a planet's atmospheric environment. To our knowledge, RATE has not previously been employed to measure the thermal effect of planetary atmospheres.

Two methods have been proposed thus far for estimating the average surface temperatures of planetary bodies without the greenhouse effect, both based on the Stefan-Boltzmann (SB) radiation law. The first and most popular approach uses the planet's global energy budget to calculate a single radiating equilibrium temperature T_{e} (a.k.a. effective emission temperature) from the spherically integrated absorbed stellar flux (e.g. Taylor 2010a; Pierrehumbert 2010; Lacis et al. 2013), i.e.

$$T_{\mathrm{e}} = \left[\frac{S\left(1-\alpha_p\right)}{4\,\varepsilon\,\sigma}\right]^{0.25} \qquad (3)$$

Here, S is the stellar irradiance (W m^{-2}) defined as the TOA shortwave flux incident on a plane perpendicular to the incoming rays, α_p is the planetary Bond albedo (decimal fraction), ε is the planet's effective long-wave emissivity (typically $0.9 \leq \varepsilon < 1.0$; in this study $\varepsilon = 0.98$), and σ = 5.6704×10^{-8} W m^{-2} K^{-4} is the SB constant. The factor 1/4 inside the parentheses serves to distribute the stellar flux from a flat surface to a sphere and arises from the fact that the surface area of a sphere is 4 times larger than the surface area of a disk with the same radius. Hence, the term $S\left(1-\alpha_p\right)/4$ represents the globally averaged shortwave flux absorbed by a planet-atmosphere system. The rationale behind Eq. (3) is a presumption that the TOA energy balance defines a baseline temperature at a certain altitude in the free atmosphere which is related to planet's mean surface temperature through the infrared optical depth of the atmosphere (Pierrehumbert 2010, 2011). Eq. (3) was introduced to planetary science in the early 1960s (Blanco and McCuskey 1961; Möller 1964) and has been widely utilized ever since to calculate the average surface temperatures of airless (or nearly airless) bodies such as Mercury, Moon, and Mars (Williams 2013) as well as to quantify the strength of the greenhouse effect of planetary atmospheres (e.g. Hansen et al. 1981; Peixoto and Oort 1992; Wallace and Hobbs 2006; Pierrehumbert 2010; Taylor 2010a; Lacis et al. 2013).

The second method aims at estimating the average surface temperature of a planet (T_{na}) in the complete absence of an atmosphere using an explicit spatial integration of the SB law over a sphere. Instead of calculating a single bulk temperature from the average absorbed shortwave flux as done in Eq. (3), this alternative approach first computes the equilibrium temperature at *every* point on the surface of an airless planet from the local absorbed shortwave flux using the SB relation, and then spherically integrates the resulting temperature field to produce a global temperature mean. While conceptually opposite to Eq. (3), this method mimics well the procedure for calculating Earth's global temperature as an area-weighted average of surface observations.

Rubincam (2004) proposed an analytic solution to the spherical integration of the SB law (his Eq. 15) assuming no heat storage by the regolith and zero thermal inertia of the ground. Volokin and ReLlez (2014) improved upon Rubincam's formulation by deriving a closed-form expression that explicitly accounts for effects of subterranean heat storage, cosmic microwave background radiation (CMBR) and geothermal fluxes on the average global surface temperature of an airless planet. The complete form of their analytic Spherical Airless-Temperature (SAT) model reads:

$$T_{\mathrm{na}} = \frac{2}{5}\left\{\frac{\left[(1-\eta_e)\,S\,(1-\alpha_e)+R_c+R_g\right]^{5/4}-\left(R_C+R_g\right)^{5/4}}{(1-\eta_e)\,S\,(1-\alpha_e)(\varepsilon\sigma)^{1/4}} + \frac{\left[0.754\,\eta_e\,S\,(1-\alpha_e)+R_c+R_g\right]^{5/4}-\left(R_C+R_g\right)^{5/4}}{0.754\,\eta_e\,S\,(1-\alpha_e)(\varepsilon\sigma)^{1/4}}\right\} \qquad (4a)$$

where $\alpha_e = 0.132$ is the effective shortwave albedo of regolith, $\eta_e = 0.00971$ is an effective ground heat storage coefficient in vacuum, $R_c = \sigma\, 2.725^4 = 3.13\times10^{-6}$ W m^{-2} is CMBR (Fixsen 2009), and R_g is a spatially homogeneous geothermal flux (W m^{-2}) emitted from the subsurface. The heat storage term η_e is defined as a fraction of the absorbed shortwave flux conducted into the regolith during daylight hours and subsequently released as heat at night. Values of α_e, η_e and ε were estimated from NASA measurements and models of the Moon (Vasavada et al. 2012; Volokin and ReLlez 2014).

Since the effect of CMBR on T_{na} is negligible for $S_o > 0.15$ W m^{-2} and the contribution of geothermal fluxes to surface temperatures is oftentimes insignificant, in most cases, one can simplify Eq. (4a) by substituting $R_c = R_g = 0$. This produces (Volokin and ReLlez 2014):

$$T_{\mathrm{na}} = \frac{2}{5}\left[\frac{S\,(1-\alpha_e)}{\varepsilon\,\sigma}\right]^{0.25}\left[(1-\eta_e)^{0.25}+0.932\,{\eta_e}^{0.25}\right] \qquad (4b)$$

where $0.932 = 0.754^{0.25}$. The complete formula (4a) only needs to be used if $S \leq 0.15$ W m^{-2} and/or if the magnitude of R_g is significantly greater than zero. For comparison, the 0.15 W m^{-2} irradiance threshold is encountered in the Solar System by bodies orbiting at 95 AU and beyond, i.e. in the region of the inner Oort cloud. Volokin and ReLlez (2014) verified Eqs. (4a) and (4b) against Moon temperature data provided by the NASA Diviner Lunar Radiometer Experiment (Paige et al. 2010; Vasavada et al. 2012). These authors also showed that accounting for the subterranean heat storage (η_e) markedly improves the accuracy and physical robustness of the SAT model compared to the original formulation by Rubincam (2004).

The conceptual difference between Eqs. (3) and (4b) is that T_{e} represents the equilibrium temperature of a black *disk* orthogonally illuminated by shortwave radiation with intensity equal to the average solar flux absorbed by a sphere having a Bond albedo α_p, while T_{na} is the area-weighted average temperature of a thermally heterogeneous airless sphere (Leconte et al. 2013; Volokin and ReLlez 2014). Due to Hölder's inequality between integrals (Beckenbach and Bellman 1983), one always finds $T_{na} << T_{\mathrm{e}}$ when using equivalent values of stellar irradiance and surface albedo in Eqs. (3) and (4b) (Volokin and ReLlez 2014).

Since regolith-covered celestial bodies with tenuous atmosphere are expected to have similar optical and thermo-physical properties of their surfaces (Volokin and ReLlez 2014), one can further simplify Eq. (4b) by combining the albedo (α_e), heat storage fraction (η_e) and emissivity (ε) into a single constant using applicable values for the Moon to obtain:

$$T_{\mathrm{na}} = 32.44\, S^{0.25} \qquad (4c)$$

Eq. (4c) was employed to calculate the 'no-atmosphere' reference temperatures of all planetary bodies in our study (see Section 2.3).

For a reference pressure we chose the gas-liquid-solid triple point of water, i.e. $P_r = 611.73$ Pa (Cengel and Turner 2004) that defines a baric threshold, below which water can only exists in a solid/vapor phase and not in a liquid form. The presence of liquid water on a planet's surface is important because (*a*) it significantly impacts the amount of atmospheric water vapor, a powerful greenhouse gas believed to control surface temperatures (e.g. Schmidt et al. 2010; Lacis et al. 2013), and (*b*) liquid water is crucial for the evolution of life as we know it. It should be pointed out that the results of our analysis are not sensitive to the particular choice of a reference-pressure value, i.e. P_r is a matter of convention.

2.2. Regression Analysis

Finding the best function to describe the observed variation of GMAT across celestial bodies requires that the π_i variables generated by DA be subjected to regression analyses. As explained in Appendix A, twelve pairs of π_i variables hereto called models were investigated. In order to ease the curve fitting and simplify the visualization of results, we utilized the natural logarithms of π_i variables rather than their absolute values, i.e. we modeled the relationship $\ln(\pi_1) = f(\ln(\pi_2))$ instead of $\pi_1 = f(\pi_2)$. In doing so we focused on monotonic functions of conservative shapes such as exponential, sigmoidal, hyperbolic, and logarithmic, for their fitting coefficients might be interpretable in physically meaningful terms. A key advantage of this type of functions (provided the existence of a good fit, of course) is that they also tend to yield reliable results outside the data range used to determine their coefficients. We specifically avoided non-monotonic functions such as polynomials because of their ability to accurately fit almost any dataset given a sufficiently large number of regression coefficients while at the same time showing a poor predictive skill beyond the calibration data range.

The following four-parameter exponential-growth function was found to best meet our criteria:

$$y = a \exp(b\, x) + c \exp(d\, x) \qquad (5)$$

where $x = \ln(\pi_2)$ and $y = \ln(\pi_1)$ are the independent and dependent variable respectively while a, b, c and d are regression coefficients. Eq. (5) was fitted to each one of the 12 planetary data sets of logarithmic π_i pairs suggested by DA using the standard method of

least squares. Predictive skills of the resulting regression models were evaluated via 3 statistical criteria: coefficient of determination (R^2), adjusted R^2, and standard error of the estimate, σ (Steel and Torrie 1960; Zwillinger 1995).

2.3. Planetary Dataset

To ensure proper application of the DA methodology we compiled a dataset of diverse planetary environments in the Solar System using the best up-to-date information available. Celestial bodies were selected for our analysis based on three criteria: (*a*) presence of a solid surface with at least traces of atmosphere, i.e. gas planets such as Jupiter and Saturn were excluded; (*b*) availability of reliable data on near-surface temperature, atmospheric composition, and total air pressure/density preferably from direct observations; and (*c*) representation of a broad range of physical environments defined in terms of TOA solar irradiance and atmospheric properties. This resulted in the selection of three planets: Venus, Earth, and Mars; and three natural satellites: Moon of Earth, Titan of Saturn, and Triton of Neptune.

Each celestial body was described by eight parameters shown in Table 2 with data sources listed in Table 3. In an effort to minimize the effect of the unforced (internal) climate variability on our temperature model, we attempted to assemble a dataset representing a 30-year observational period, i.e. from 1981 to 2010. Thus, Voyager measurements of Titan from early 1980s suggested an average surface temperature of 94 ± 0.7 K (Atreya et al. 2009). Subsequent observations by the Cassini mission between 2005 and 2010 indicated a mean global temperature of 93.4 ± 0.6 K for that moon (Jennings et al. 2009; Cottini et al. 2012). Since Saturn's orbital period equals 29.45 Earth years, we averaged the above global temperature values to arrive at 93.7 ± 0.6 K for Titan's long-term GMAT. Similarly, data obtained in late 1970s by the Viking Landers on Mars were combined with more recent remote observations by the Mars Global Surveyor (MGS) spacecraft to derive representative estimates of GMAT and atmospheric surface pressure for the Red Planet. Some parameter values reported in the literature did not meet our stringent criteria for global representativeness and/or physical plausibility and were recalculated using available observations as described below.

The mean solar irradiances of all bodies were computed as $S = S_o\ r_{\mathrm{au}}{}^{-2}$, where r_{au} is the body's average distance (semi-major axis) to the Sun (AU) and S_o = 1,360.9 W m^{-2} is Earth's new lower irradiance at 1 AU according to recent satellite observations reported by Kopp and Lean (2011). Due to a design flaw in earlier spectrometers, the solar irradiance at Earth's distance has been overestimated by ≈5 W m^{-2} prior to 2003 (Kopp and Lean 2011).

Table 2 Planetary data set used in the Dimensional Analysis and compiled from sources listed in Table 3. See text for details about the computational methods employed for some parameters. The estimation of Mars' GMAT and its average surface atmospheric pressure are discussed in Appendix B.

Parameter	Venus	Earth	Moon	Mars	Titan	Triton
Average distance to the Sun, r_{au} (AU)	0.7233	1.0	1.0	1.5237	9.582	30.07
TOA average solar irradiance, S (W m^{-2})	2,601.3	1,360.9	1,360.9	586.2	14.8	1.5
Bond albedo, α_p (decimal fraction)	0.900	0.294	0.136	0.250	0.265	0.650
Global average total atmospheric surface pressure, P (Pa)	9,300,000.0 ± 100,000	98,550.0 ± 6.5	2.96×10^{-10} $\pm 10^{-9}$	685.4 ± 14.2	146,700.0 ± 100	4.0 ±1.2
Average near-surface atmospheric density, ρ (kg m^{-3})	65.868 ± 0.44	1.193 ± 0.002	2.81×10^{-15} $\pm 9.4\times10^{-15}$	0.019 $\pm 3.2\times10^{-4}$	5.161 ± 0.03	3.45×10^{-4} $\pm 9.2\times10^{-5}$
Chemical composition of the lower atmosphere (% of volume)	96.5 CO_2 3.48 N_2 0.02 SO_2	77.89 N_2 20.89 O_2 0.932 Ar 0.248 H_2O 0.040 CO_2	26.7 ^{4}He 26.7 ^{20}Ne 23.3 H_2 20.0 ^{40}Ar 3.3 ^{22}Ne	95.32 CO_2 2.70 N_2 1.60 Ar 0.13 O_2 0.08 CO 0.021 H_2O	95.1 N_2 4.9 CH_4	99.91 N_2 0.060 CO 0.024 CH_4
Molar mass of the lower atmosphere, M (kg mol^{-1})	0.0434	0.0289	0.0156	0.0434	0.0274	0.0280
Observed GMAT, T_s (K)	737.0 ± 3.0	287.4 ± 0.5	197.35 ± 0.9	190.56 ± 0.7	93.7 ± 0.6	39.0 ± 1.0

Consequently, our calculations yielded slightly lower irradiances for some bodies such as Venus and Mars compared to previously published values. Our decision to recalculate S was based on the assumption that orbital distances of planets are known with much greater accuracy than TOA solar irradiances. Hence, a correction made to Earth's irradiance requires adjusting the 'solar constants' of other planets as well.

We found that published data for the mean global temperature and the average surface atmospheric pressure of Mars were either improbable or too uncertain to be useful for our analysis. Existing sources report Mars' GMAT anywhere between 200 K and 240 K with

Table 3 Literature sources of the planetary data presented in Table 2.

Planetary Body	Information Sources
Venus	Fegley et al. (1997); Basilevsky and Head (2003); Mallama et al. (2006); Basilevsky and McGill (2007); Williams (2014); NASA Solar System Exploration (2014).
Earth	Jones et al. (1999); Trenberth and Smith (2005); Smith et al. (2008); Kopp and Lean (2011); Stephens et al. (2012); Wild et al. (2013); Williams (2014); NOAA National Climatic Data Center (2014); Stephens et al. (2015).
Moon	Keihm (1984); Vasavada et al. (1999); Lucey et al. (2006); Matthews (2008); Vasavada et al. (2012); Williams (2014); NASA Solar System Exploration (2014); Volokin and ReLlez (2014).
Mars	Hinson et al. (2004); Hinson (2006); Williams (2014); NASA Solar System Exploration (2014); Kemppinen et al. (2013); Appendix B.
Titan	Younkin (1974); Hanel et al. (1985); Neff et al. (1985); Fulchignoni et al. (2005); Niemann et al. (2005); Griffith (2007); Mitri et. al (2007); Jennings et al. (2009); Atreya et al. (2009); Li et al. (2011); Cottini et al. (2012); Schinder et al. (2012); Williams (2014).
Triton	Nelson et al. (1990); Elliot et al. (1998); Lellouch et al. (2010); NASA Solar System Exploration (2014).

the most frequently quoted values in the range 210 – 220 K (Smil 2003; Vázquez and Hanslmeier 2006; Barlow 2008; Rapp 2008; Taylor 2010; Lacis et al. 2013; Lissauer and Pater 2013; Williams 2014). However, in-situ measurements by Viking Landers suggest that the average surface air temperature at a low-elevation site in the Martian subtropics does not exceed 207 K during the warmer summer-fall season (Appendix B). Therefore, the Red Planet's GMAT must be lower than 207 K. The Viking record also indicates that diurnal average temperatures above 210 K can only occur on Mars during the summer season. Hence, such values are likely significantly higher than the actual mean annual temperature at any Martian latitude. The surface atmospheric pressure on Mars varies appreciably with season and location. Its global average value has previously been reported between 600 Pa and 700 Pa (Jakosky and Phillips 2001; Catling and Leovy 2007; Barlow 2008; Taylor 2010b; Williams 2013; Lacis et al. 2013), a range that was too broad for the target precision of our study. Hence, our decision to calculate new global means of near-surface temperature and air pressure for the Red Planet via a thorough analysis of available data from remote-sensing and in-situ observations. Appendix B describes our computational procedure with the results presented in Table 2.

Moon's GMAT was also not readily extractable from the existing literature. Although lunar temperatures have been measured for over 50 years both remotely (via Earth-based telescopes or by instruments aboard lunar orbiters) and in situ (by the Surveyor and Apollo landing mission) (Paige et al. 2010), most studies focus on observed temperature extremes across the lunar surface (e.g. Lucey et al. 2006) and rarely discuss Moon's average global temperature. Current GMAT estimates for the Moon cluster around two narrow ranges: 250–255 K and 269 –271 K (e.g. Williams 2013). A careful examination of published data reveals that the 250–255 K range is based on subterranean heat-flow measurements conducted at depths between 80 and 140 cm at the Apollo 15 and 17 landing sites located respectively at 26^{o} N; 3.6^{o} E and 20^{o} N; 30.6^{o} E (Vaniman et al. 1991). Due to a strong dependence of the lunar regolith thermal conductivity on temperature in the topmost 1-2 cm soil, Moon's average diurnal temperature steadily increases with depth. According to Apollo measurements, the mean daily temperature at 35 cm belowground is 40 –45 K higher than that at the lunar surface (Vaniman et al. 1991). The diurnal temperature fluctuations completely vanish below a depth of 80 cm. At 100-cm depth, the temperature of lunar regolith ranged from 250.7 K to 252.5 K at the Apollo 15 site and between 254.5 K and 255.5 K at the Apollo 17 site (see Figure 3.9 in Vaniman et al. 1991). Hence, reported Moon average temperatures between 250 K and 255 K do not describe surface conditions. Moreover, since measured in the lunar subtropics, such temperatures do not likely even represent Moon's global thermal environment at these depths. On the other hand, frequently quoted Moon global temperatures of ~270 K are not based on actual surface measurements but calculated from Eq. (3) instead. However, Volokin and ReLlez (2014) demonstrated that Eq. (3) yields non-physical results for a sphere that are ~37% higher than the actual mean global temperature of the surface. Hence, in this study, we employ the 197.35 K spherical estimate of Moon's GMAT obtained by Volokin and ReLlez (2014) using output from a detailed NASA thermo-physical model of the lunar regolith validated against Diviner observations (Vasavada et al. 2012).

Surprisingly, many publications also do not report a correct value for Earth's mean global temperature. Terrestrial climate studies typically focus on temperature anomalies and if Earth's GMAT is ever mentioned, it is often loosely quoted as 15 C (~288 K) (e.g. Hansen et al. 1981; Peixoto and Oort 1992; Wallace and Hobbs 2006; Lacis et al. 2013). However, observations in the HadCRUT4 dataset of the UK Met Office's Hadley Centre (Jones et al. 1999; Morice et al. 2012) and in the Global Historical Climatology Network of the NOAA National Center for Environmental Information (formerly the National Climatic Data Center) (Peterson and Vose 1997; Smith and Reynolds 2005; Smith et al. 2008) indicate that, between 1981 and 2010, Earth's mean annual surface air temperature was 287.4 K (14.3 C) ± 0.5 K. For comparison, Earth's GMAT over the past 17 years (1998-2015), a period of a relatively stable climate, has been 287.6 ± 0.5 K. Some recent studies acknowledge these more accurate lower values of Earth's absolute global temperature (e.g. Hansen et al. 2013). For the Earth's mean surface atmospheric pressure we adopted the 98.55 kPa estimate by

Trenberth and Smith (2005), which takes into account the average elevation of continental landmasses above sea level and is, therefore**,** slightly lower than the typical sea-level pressure of ~101 kPa.

The average near-surface atmospheric densities (ρ, kg m^{-3}) of planetary bodies were computed from reported means of total atmospheric pressure (P), molar mass (M, kg mol^{-1}) and temperature (T_s) using the Ideal Gas Law, i.e.

$$\rho = \frac{P\,M}{R\,T_s} \qquad (6)$$

where R = 8.31446 J mol^{-1} K^{-1} is the universal gas constant. This re-calculation was intended to make atmospheric densities physically consistent with independent data on pressure and temperature utilized in our study. The resulting ρ values for individual planetary bodies are similar to previously published data. Standard errors of the air-density estimates were calculated from reported errors of P and T_s for each body using Eq. (6).

Data in Table 2 were harnessed to calculate several intermediate variables and all dimensionless π_i products necessary for the regression analyses. The results from these calculations are shown in Table 4. Greenhouse gases in planetary atmospheres represented by the major constituents, i.e. carbon dioxide (CO_2), methane (CH_4) and water vapor (H_2O), were collectively quantified via three bulk parameters: average molar mass (M_{gh}, kg mol^{-1}), combined partial pressure (P_{gh}, Pa) and combined partial density (ρ_{gh}, kg m^{-3}). These parameters were computed from reported volumetric concentrations of individual greenhouse gases (C_x, %) and data on total atmospheric pressure and density using the formulas:

$$M_{gh} = (0.044\,C_{\mathrm{CO2}} + 0.016\,C_{\mathrm{CH4}} + 0.018\,C_{\mathrm{H2O}})/C_{gh} \qquad (7)$$

$$P_{gh} = P\,(0.01\,C_{gh}) \qquad (8)$$

$$\rho_{gh} = \rho\,(0.01\,C_{gh})(M_{gh}/M) \qquad (9)$$

where $C_{gh} = C_{\mathrm{CO2}} + C_{\mathrm{CH4}} + C_{\mathrm{H2O}}$ is the total volumetric concentration of major greenhouse gases (%). The reference temperatures T_{e} and T_{na} were computed from Eqs. (3) and (4c) respectively.

Table 4 Intermediate variables and dimensionless products computed from data in Table 2 and required for the regression analysis. Equations for computing intermediate variables are shown in parentheses. Reference pressure is set to the barometric triple point of water, i.e. $P_r = 611.73$ Pa.

Intermediate Variable or Dimensionless Product	Venus	Earth	Moon	Mars	Titan	Triton
Average molar mass of greenhouse gases, M_{gh} (kg mol^{-1}) (Eq. 7)	0.0440	0.0216	0.0	0.0440	0.0160	0.0160
Near-surface partial pressure of greenhouse gases, P_{gh} (Pa) (Eq. 8)	8,974,500.0 ± 96,500	283.8 ± 0.02	0.0	667.7 ± 13.8	7,188.3 ± 4.9	9.6×10^{-4} ± 2.9×10^{-4}
Near-surface density of greenhouse gases, ρ_{gh} (kg m^{-3}) (Eq. 9)	64.441 ±0.429	2.57×10^{-3} ±4.3×10^{-6}	0.0	0.018 ± 3.1×10^{-4}	0.148 ± 8.4×10^{-4}	4.74×10^{-8} ± 1.3×10^{-8}
Radiating equilibrium temperature, T_e (K) (Eq. 3)	185.0	256.4	269.7	210.9	83.6	39.2
Mean airless spherical temperature, T_na (K) (Eq. 4c)	231.7	197.0	197.0	159.6	63.6	35.9
T_s/T_e	3.985 ± 0.016	1.121 ± 0.002	0.732 ± 0.003	0.904 ± 0.003	1.120 ± 0.007	0.994 ± 0.026
T_s/T_na	3.181 ± 0.013	1.459 ± 0.002	1.002 ± 0.004	1.194 ± 0.004	1.473 ± 0.009	1.085 ± 0.028
$\ln(T_s/T_\mathrm{e})$	1.3825 ± 0.0161	0.1141 ± 0.0019	-0.3123 ± 0.0033	-0.1013 ± 0.0033	0.1136 ± 0.0071	-6.03×10^{-3} ± 0.0252
$\ln(T_s/T_\mathrm{na})$	1.1573 ± 0.0129	0.3775 ± 0.0025	1.59×10^{-3} ± 0.0046	0.1772 ± 0.0044	0.3870 ± 0.0094	0.082 ± 0.0275
$\ln\left[{P_{gh}}^3/(\rho_{gh}\ S^2)\right]$	28.1364	8.4784	Undefined	10.7520	23.1644	-4.7981
$\ln\left[P^3/(\rho_{gh}\ S^2)\right]$	28.2433	26.0283	$+\infty$	10.8304	32.2122	20.2065
$\ln\left[{P_{gh}}^3/(\rho\ S^2)\right]$	28.1145	2.3370	Undefined	10.7396	19.6102	-13.6926
$\ln\left[P_{gh}/P_r\right]$	9.5936	-0.7679	Undefined	0.0876	2.4639	-13.3649
$\ln[P^3/(\rho\ S^2)]$	28.2214	19.8869	-46.7497	10.8180	28.6580	11.3120
$\ln(P/P_r)$	9.6292 ± 5.1027	5.0820 ± 0.0106	-28.3570 ± 2×10^{-12}	0.1137 ± 0.0229	5.4799 ± 0.1514	-5.0300 ± 0.0020

3. Results and Discussion

Function (5) was fitted to each one of the 12 sets of logarithmic π_i pairs generated by Eqs. (1) and (2) and shown in Table 4. Figures 1 and 2 display the resulting curves of individual regression models with planetary data plotted in the background for reference. Table 5 lists the statistical scores of each non-linear regression. Model 12 depicted in Fig. 2f has the highest R^2 = 0.9999 and the lowest standard error $\sigma = 0.0078$ among all regressions. Model 1 (Fig. 1a) provides the second best fit with R^2 = 0.9844 and $\sigma = 0.1529$. Notably, Model 1 has almost a 20-time larger standard error than Model 12. Figure 3 illustrates the difference in predictive skills between the two top-performing models (1 and 12) employing linear vertical axes for clarity. The results presented in Table 5 indicate that Model 12 possesses an explanatory power and a descriptive accuracy surpassing those of the other models by a wide margin.

Since Titan and Earth nearly overlap on the logarithmic scale of Fig. 2f, we experimented with an alternative regression for Model 12 that excluded Titan from the input dataset. Remarkably, this new curve had R^2 = 1.0 and $\sigma = 0.0009$. Although the two regression equations produce similar results over most of the pressure range, we chose the one without Titan as final for Model 12 based on the assumption that Earth's GMAT is likely known with a much greater certainty than Titan's mean annual temperature. Taking an antilogarithm of the final regression equation (excluding Titan) yielded the following expression for Model 12:

$$\frac{T_s}{T_{\mathrm{na}}} = \exp\left[0.174205\left(\frac{P}{P_r}\right)^{0.150263} + 1.83121 \times 10^{-5}\left(\frac{P}{P_r}\right)^{1.04193}\right] \qquad (10a)$$

The regression coefficients are intentionally provided in full precision in order to facilitate replication of our results by other researchers and to allow an accurate calculation of RATE (i.e. the T_s/T_{na} ratio) given the strong non-linearity of the relationship. Figure 4 depicts Eq. (10a) as a dependence of RATE on the average surface air pressure. Superimposed on the graph are the six planetary bodies from Table 4 along with their uncertainty estimates. Substituting the reference temperature T_{na} in Eq. (10a) with its equivalent from Eq. (4c) and solving for T_s produces the final formula for estimating GMAT of rocky planets as a function of just two forcing variables: TOA stellar irradiance (S) and mean surface atmospheric pressure (P), i.e.

$$T_s = 32.44\, S^{0.25} \exp\left[0.174205\left(\frac{P}{P_r}\right)^{0.150263}\right] \exp\left[1.83121 \times 10^{-5}\left(\frac{P}{P_r}\right)^{1.04193}\right] \qquad (10b)$$

Note that if $S \leq 0.15$ W m^{-2} and/or the geothermal flux R_g is significantly greater than zero, one must employ Eq. (4a) to compute T_{na} instead of Eq. (4c). The final model can also be

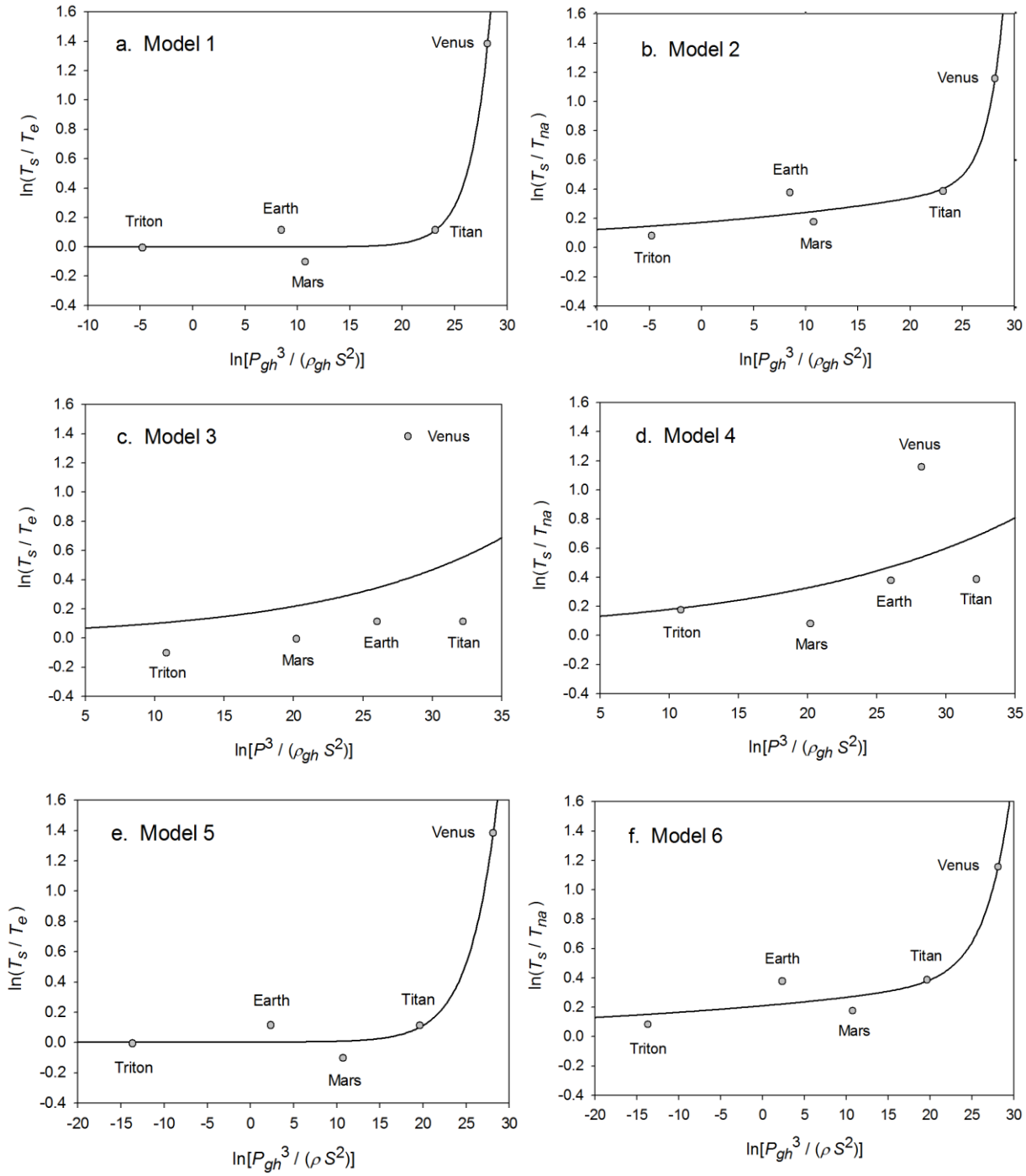

Figure 1 Relative atmospheric thermal enhancement (T_s/T_r) as a function of various dimensionless forcing variables generated by DA using data on solar irradiance, near-surface partial pressure/density of greenhouse gases, and total atmospheric pressure/density from Table 4. Panels *a* through *f* depict six regression models suggested by DA with the underlying celestial bodies plotted in the background. Each pair of horizontal graphs shows different reference temperatures (T_r) defined as either $T_r = T_e$ (left) or $T_r = T_{na}$ (right).

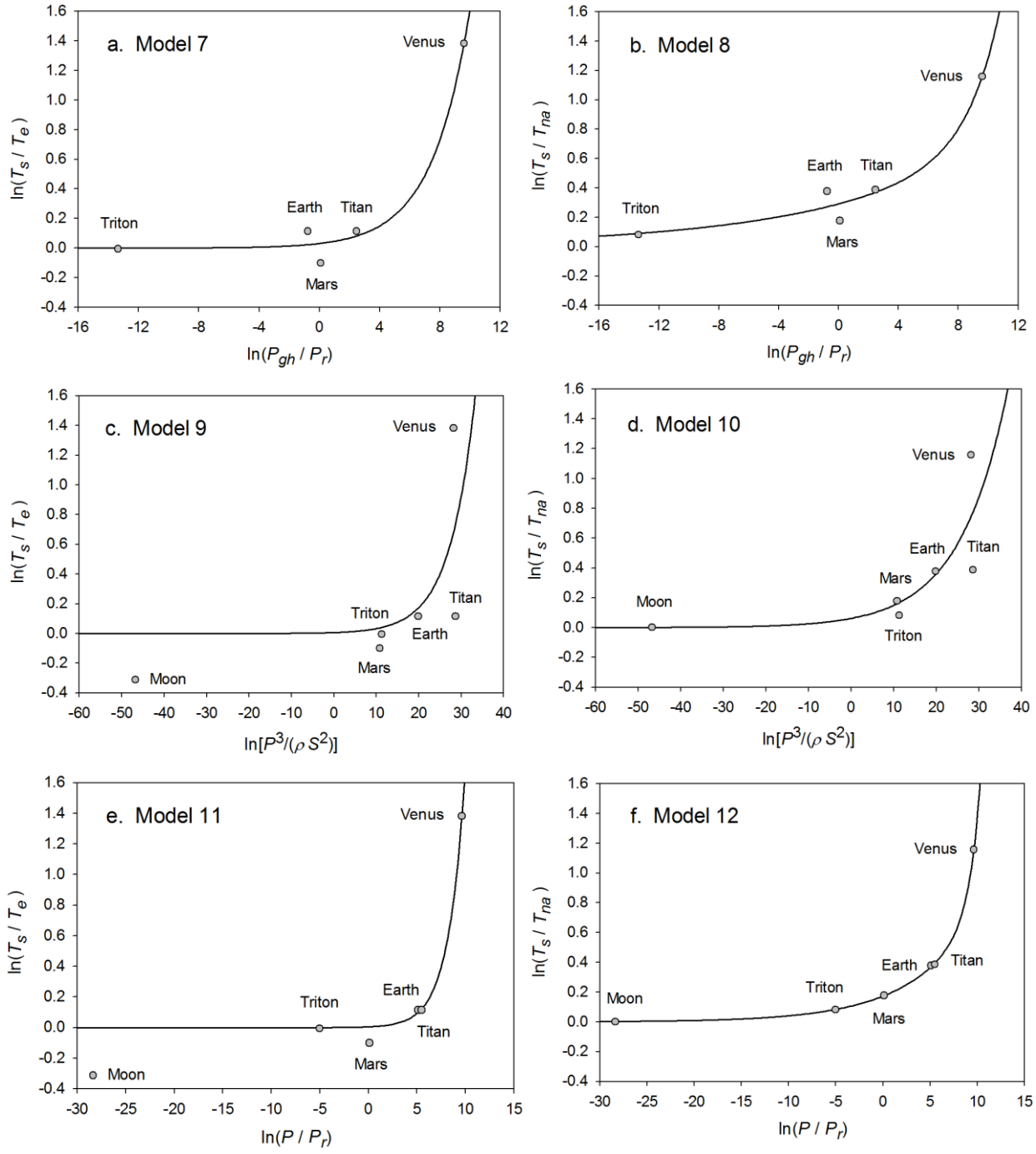

Figure 2 The same as in Fig. 1 but for six additional regression models (panels *a* through *f*)

Table 5 Performance statistics of twelve regression models suggested by the Dimensional Analysis. Statistical scores refer to the model logarithmic forms shown in Figs. 1 and 2.

No.	Functional Model	Coefficient of Determination (R^2)	Adjusted R^2	Standard Error σ
1	$\frac{T_s}{T_e} = f\left(\frac{{P_{gh}}^3}{\rho_{gh}\ S^2}\right)$	0.9844	0.9375	0.1529
2	$\frac{T_s}{T_{na}} = f\left(\frac{{P_{gh}}^3}{\rho_{gh}\ S^2}\right)$	0.9562	0.8249	0.1773
3	$\frac{T_s}{T_e} = f\left(\frac{P^3}{\rho_{gh}\ S^2}\right)$	0.1372	-2.4511	1.1360
4	$\frac{T_s}{T_{na}} = f\left(\frac{P^3}{\rho_{gh}\ S^2}\right)$	0.2450	-2.0200	0.7365
5	$\frac{T_s}{T_e} = f\left(\frac{{P_{gh}}^3}{\rho\ S^2}\right)$	0.9835	0.9339	0.1572
6	$\frac{T_s}{T_{na}} = f\left(\frac{{P_{gh}}^3}{\rho\ S^2}\right)$	0.9467	0.7866	0.1957
7	$\frac{T_s}{T_e} = f\left(\frac{P_{gh}}{P_r}\right)$	0.9818	0.9274	0.1648
8	$\frac{T_s}{T_{na}} = f\left(\frac{P_{gh}}{P_r}\right)$	0.9649	0.8598	0.1587
9	$\frac{T_s}{T_e} = f\left(\frac{P^3}{\rho\ S^2}\right)$	0.4488	-0.3780	0.7060
10	$\frac{T_s}{T_{na}} = f\left(\frac{P^3}{\rho\ S^2}\right)$	0.6256	0.0639	0.4049
11	$\frac{T_s}{T_e} = f\left(\frac{P}{P_r}\right)$	0.9396	0.8489	0.2338
12	$\frac{T_s}{T_{na}} = f\left(\frac{P}{P_r}\right)$	0.9999	0.9997	0.0078

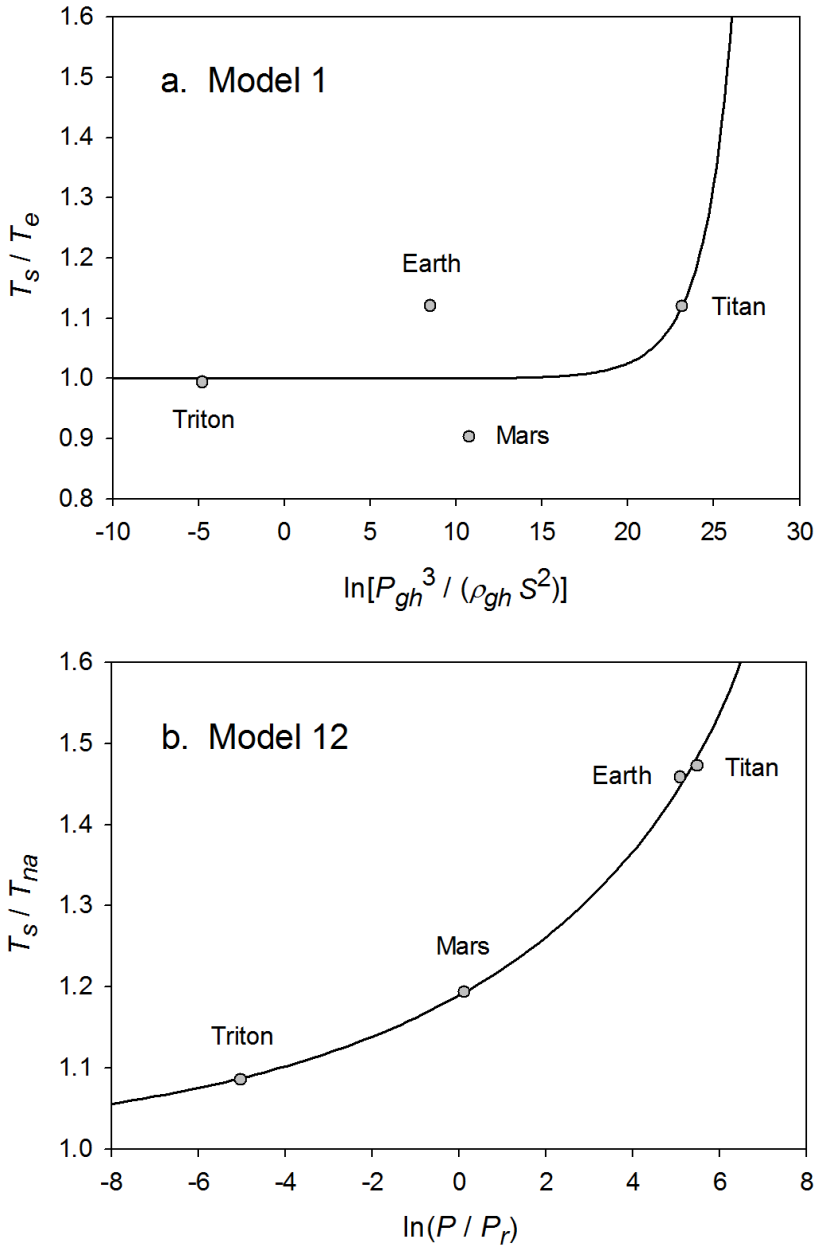

Figure 3 Comparison of the two best-performing regression models according to statistical scores presented in Table 5. Vertical axes use linear scale to better illustrate the difference in skills between the models.

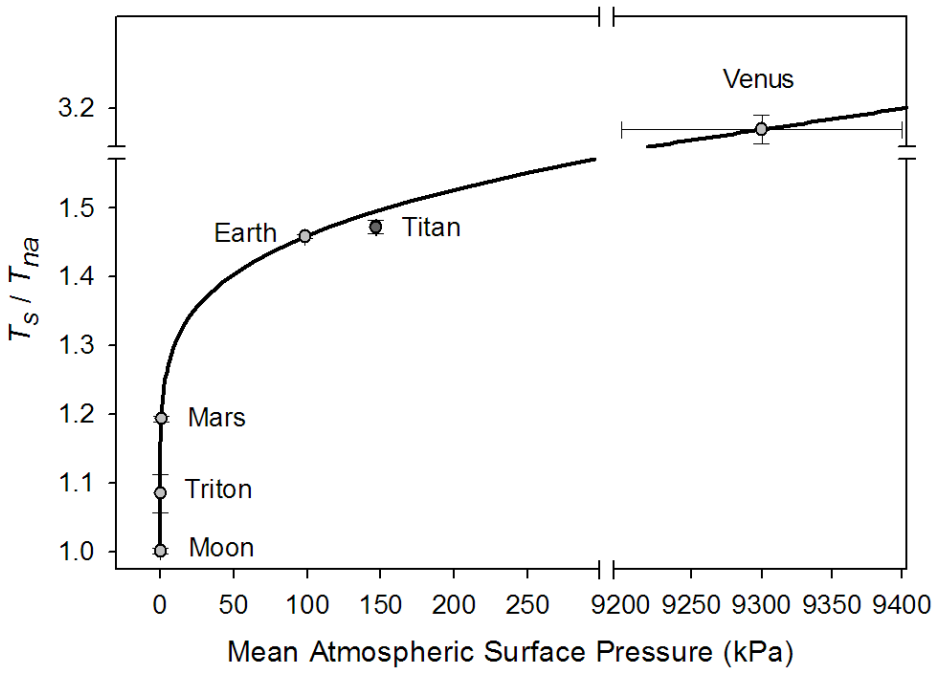

Figure 4 Dependence of the relative atmospheric thermal enhancement (T_s/T_{na}) on mean surface air pressure according to Eq. (10a) derived from data representing a broad range of planetary environments in the Solar System. Saturn's moon Titan has been excluded from the regression analysis leading to Eq. (10a). Error bars of some bodies are not clearly visible due to their small size relative to the scale of the axes. See Table 2 for the actual error estimates.

written in terms of T_s as a function of planet's distance to the Sun r_{au} (AU) and surface atmospheric pressure by replacing $S^{0.25}$ in Eq. (10b) with $(6.0737\ {r_{\mathrm{au}}}^{-0.5})$.

3.1. Features of the New Planetary Temperature Model

3.1.1 Accuracy and Scope

Fig. 5 portrays the residuals between modeled and observed absolute planetary temperatures (from Eq. 10b and Table 2, respectively). For celestial bodies participating in the regression analysis (i.e. Venus, Earth, Moon, Mars and Triton), the maximum model error does not exceed 0.17 K and is well within the uncertainty of observations. The error for Titan, an independent data point, is 1.45 K or 1.5% of that moon's current best-known GMAT (93.7 K). Eq. (10b) produces 95.18 K for Titan at Saturn's semi-major axis (9.582 AU) corresponding to a solar irradiance S = 14.8 W m^{-2}. This estimate is virtually identical to the 95 K (-178 C) average surface temperature reported for Titan by the NASA JPL Voyager Mission (2014) web site. The Voyager spacecraft 1 and 2 reached Saturn and its moons in November 1980 and August 1981 respectively, when the gas giant was near its semi-major axis, i.e. at a distance between 9.52 AU and 9.60 AU from the Sun (NASA JPL Ephemeris

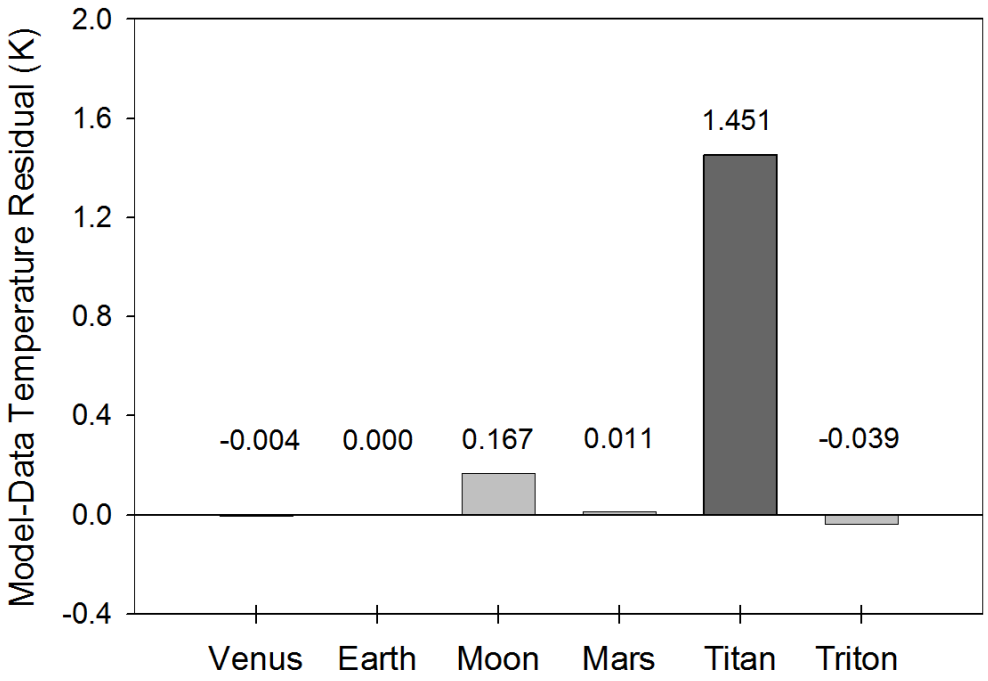

Figure 5 Absolute differences between predicted average global surface temperatures (Eq. 10b) and observed GMATs (Table 2) for the studied celestial bodies. Titan represents an independent data point, since it was excluded from the non-linear regression analysis leading to Eq. (10a).

2014). Data acquired by Voyager 1 suggested an average surface temperature of 94 ± 0.7 K on Titan, while Voyager 2 indicated a temperature close to 95 K (Atreya et al. 2009). Measurements obtained between 2005 and 2010 by the Cassini-Huygens mission revealed T_s ≈ 93.4 ± 0.6 K (Jennings et al. 2009; Cottini et al. 2012). Using Saturn's perihelion (9.023 AU) and aphelion (10.05 AU) one can compute Titan's TOA solar irradiance at the closest and furthest approach to the Sun, i.e. 16.7 W m^{-2} and 13.47 W m^{-2} respectively. Inserting these values into Eq. (10b) produces the expected upper and lower limit of Titan's mean global surface temperature according to our model, i.e. 92.9 K ≤ T_s ≤ 98.1 K. Notably this range encompasses all current observation-based estimates of Titan's GMAT. Since both Voyager and Cassini mission only covered periods that are shorter than a Titan season (Saturn's orbital period is 29.45 Earth years), the available measurements might not well represent that moon's annual thermal cycle. In addition, due to thermal inertia, Titan's average surface temperature likely lags variations of the TOA solar irradiance caused by Saturn's orbital eccentricity. Thus, the observed 1.45 K discrepancy between our model prediction and Titan's current best-known GMAT seems to be within the range of plausible global temperature variations on that moon. Hence, further observations are needed to more precisely constrain Titan's long-term GMAT.

Measurements conducted by the Voyager spacecraft in 1989 indicated a global mean temperature of 38 ± 1.0 K and an average atmospheric pressure of 1.4 Pa at the surface of

Triton (Lellouch et al. 2010; see also the NASA Voyager web page for Triton at http://voyager.jpl.nasa.gov/science/neptune_triton.html). Even though Eq. (10a) is based on slightly different data for Triton (i.e. T_s = 39 ±1.0 K and P = 4.0 Pa) obtained by more recent stellar occultation measurements (Lellouch et al. 2010), employing the Voyager-reported pressure in Eq. (10b) produces T_s = 38.5 K for Triton's GMAT, a value well within the uncertainty of the 1989 temperature measurements.

The above comparisons indicate that Eq. (10b) rather accurately reproduces the observed variation of mean surface temperatures across a wide range of planetary environments defined in terms of solar irradiance (from 1.5 W m^{-2} to 2,602 W m^{-2}), total atmospheric pressure (from near vacuum to 9,300 kPa), and greenhouse-gas concentrations (from 0.0% to over 96% per volume). While true that Eq. (10a) is only based on data from 6 planetary bodies, one should keep in mind that these represent *all* objects in the Solar System meeting our criteria about the quality of available data discussed in Section 2.3. The fact that only one of the investigated twelve non-linear regressions yielded a really tight relationship suggests that Model 12 might be describing a macro-level thermodynamic property of planetary atmospheres heretofore unbeknown to science. A function of such predictive skill spanning the breadth of the Solar System may not be just a result of chance. Indeed, complex natural systems consisting of myriad interacting agents have been known to exhibit emergent behaviors at higher levels of hierarchical organization that are amenable to accurate modeling using top-down statistical approaches (e.g. Stolk et al. 2003). Eq. (10) also displays several other characteristics that lend further support to the above conjecture.

3.1.2. Robustness

Model robustness defines the degree to which a statistical relationship would hold when recalculated using a different dataset. To test the robustness of Eq. (10a) we performed an alternative regression analysis that excluded Earth and Titan from the input data and only utilized logarithmic pairs of T_s/T_{na} and P/P_r for Venus, the Moon, Mars and Triton from Table 4. The objective of this test was to evaluate how well the resulting new regression equation could predict the observed mean surface temperatures of Earth and Titan. Since these two bodies occupy a highly non-linear region of Model 12 (Fig. 2f), eliminating them from the regression analysis would leave a key portion of the curve poorly defined. As in all previous regressions, function (5) was fitted to the incomplete dataset (which excluded Earth and Titan) yielding the following expressions:

$$\frac{T_s}{T_{\mathrm{na}}} = \exp\left[0.174222\left(\frac{P}{P_r}\right)^{0.150275} + 5.25043 \times 10^{-15}\left(\frac{P}{P_r}\right)^{3.32375}\right] \quad (11a)$$

$$T_s = 32.44\, S^{0.25} \exp\left[0.174222\left(\frac{P}{P_r}\right)^{0.150275}\right] \exp\left[5.25043 \times 10^{-15}\left(\frac{P}{P_r}\right)^{3.32375}\right] \quad (11b)$$

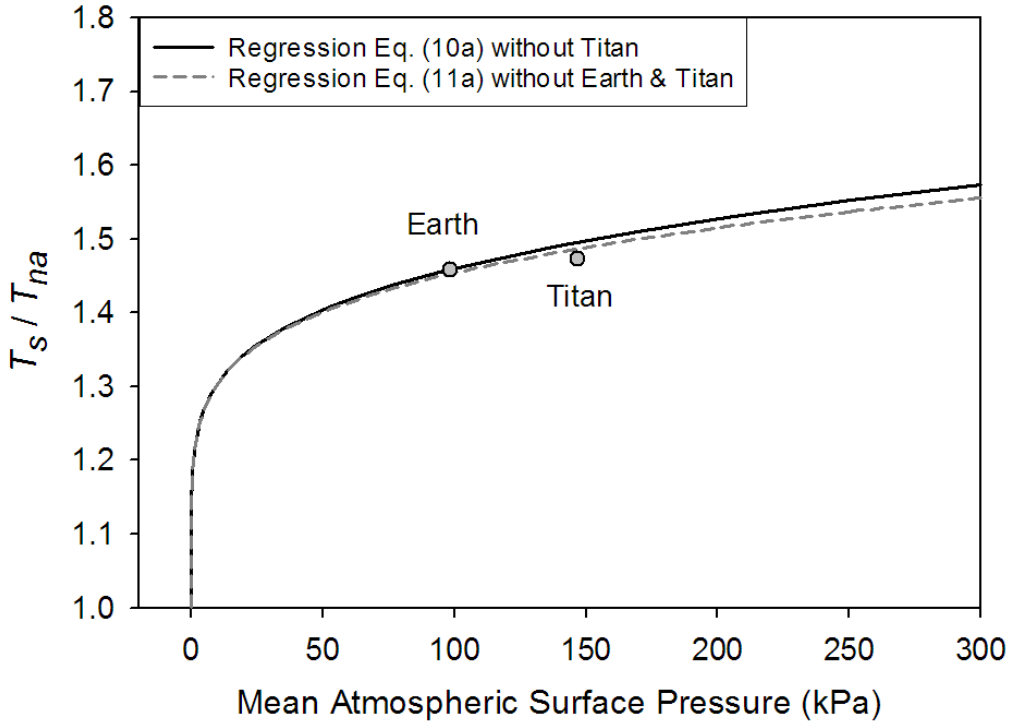

Figure 6 Demonstration of the robustness of Model 12. The solid black curve depicts Eq. (10a) based on data from 5 celestial bodies (Venus, Earth, Moon, Mars and Triton). The dashed dark-grey curve portrays Eq. (11a) derived from data of only 4 bodies (Venus, Moon, Mars and Triton) while excluding Earth and Titan from the regression analysis. Eq. (11b) predicts the observed GMATs of Earth and Titan with a better accuracy than 99%.

In comparing Eqs. (11) and (10) it is evident that the regression coefficients in the first exponent are almost identical between the two formulas. This exponent term dominates the $T_s - P$ relationship over the pressure range 0 - 400 kPa accounting for more than 97.5% of predicted temperature values. The regression coefficients of the second exponent differ somewhat between the two models causing a divergence in predicted T_s/T_{na} ratios over the pressure interval 400 –9,100 kPa. The two models converge again between 9,000 kPa and 9,300 kPa. Fig. 6 illustrates the similarity of responses between Eqs. (10a) and (11a) over the pressure range 0–300 kPa with Earth and Titan plotted in the foreground for reference.

Eq. (11b) reproduces the observed average global surface temperature of Earth with an error of 0.4% (-1.0 K) and that of Titan with an error of 1.0% (+0.9 K). For Titan, the error of Eq. (11b) is even slightly smaller than that of the original Eq. (10b). The ability of Model 12 to predict Earth's GMAT with an accuracy of 99.6% using a relationship inferred from disparate planetary environments such as those found on Venus, Moon, Mars and Triton indicates that this model is statistically robust and the Earth temperature is a part of a physical continuum well described by Eq. (10a).

The above characteristics of Eq. (10), i.e. dimensional homogeneity, high predictive accuracy, broad scope of applicability and statistical robustness, suggest that it represents an *emergent macro-level* temperature model of potential theoretical significance deserving further investigation. This conclusion is also indirectly supported by qualitative similarities between Eq. (10a) and some well-known simpler pressure-temperature relationships.

3.1.3. Similarity of Model 12 to Poisson's Formula and the SB Radiation Law

The functional response of Eq. (10a) portrayed in Fig. 4 closely resembles the shape of the dry adiabatic temperature curve in Fig. 7a described by the Poisson formula derived from the First Law of Thermodynamics and the Ideal Gas Law (e.g. Wallace and Hobbs 2006, p. 78), i.e.

$$\frac{T}{T_o} = \left(\frac{p}{p_o}\right)^{R/c_p} \qquad (12)$$

Here, T_o and p_o are reference values of temperature and pressure at the surface, while T and p are corresponding scalars in the free atmosphere, and c_p is the molar heat capacity of air (J mol^{-1} K^{-1}). For Earth's atmosphere, $R/c_p = 0.286$.

Eq. (10a) is structurally similar to Eq. (12) in a sense that both expressions relate a temperature ratio to a pressure ratio, or more precisely, a relative thermal enhancement to a ratio of forces. However, while the Poisson formula produces $0 \leq T/T_o \leq 1.0$, Eq. (10a) yields $T_s/T_{\mathrm{na}} \geq 1.0$. In other words, the reference pressure and temperature in the Poisson formula define the scalars' *upper* bounds, while reference parameters in Eq. (10a) determine the scalars' *lower* limits. This key difference between the two models stems from the fact that Eq. (12) describes vertical changes of temperature in a *free* dry atmosphere induced by a gravity-controlled pressure gradient, while Eq. (10) predicts the equilibrium response of a planet's global surface air temperature to variations in total atmospheric pressure. In a sense, Eq. (10b) could be viewed as a predictor of the reference temperature T_o in the Poisson formula. Thus, while qualitatively similar, Eqs. (10a) and (12) are quantitatively very different. Both functions describe effects of pressure on temperature but in the context of disparate physical systems. This means that estimates obtained from Eq. (10) are not comparable to and should not be confused with results inferred from the Poisson formula. For example, unlike Eq. (12), Eq. (10) cannot be expected to predict temperature lapse rates and/or vertical temperature profiles within a planetary atmosphere. Furthermore, Eq. (10) represents a top-down empirical model that implicitly accounts for a multitude of thermodynamic/radiative effects and feedbacks in the real climate system, while the Poisson formula being derived from the Ideal Gas Law only describes pressure-induced temperature changes in a homogeneous mixture of dry gases without any implicit or explicit consideration of planetary-scale climate regulators such as latent heat transport and cloud radiative forcing.

Eq. (10a) also shows an intriguing similarity to the SB law relating the equilibrium skin temperature (T_b, K) of an isothermal blackbody to the electro-magnetic radiative flux (I, W m^{-2}) absorbed (emitted) by the body's surface, i.e. $T_b = (I/\sigma)^{0.25}$. Dividing each side of this fundamental relationship by the irreducible temperature of deep Space T_c = 2.725 K and its causative CMBR R_c = 3.13×10^{-6} W m^{-2} respectively yields $T_b/T_c = (I/R_c)^{0.25}$. Further, expressing the radiative fluxes I and R_c on the right-hand side as products of photon pressure and the speed of light (c, m s^{-1}) in vacuum, i.e. $I = c\,P_{ph}$ and $R_c = c\,P_c$, leads to the following alternative form of the SB law:

$$\frac{T_b}{T_c} = \left(\frac{P_{ph}}{P_c}\right)^{0.25} \qquad (13)$$

where P_c = 1.043×10^{-14} Pa is the photon pressure of CMBR. Clearly, Eq. (10a) is analogous to Eq. (13) while the latter is structurally identical to the Poisson formula (12). Fig. 7b depicts Eq. (13) as a dependence of the T_b/T_c ratio on photon pressure P_{ph}. It is evident from Figs. 4 and 7 that formulas (10a), (12) and (13) describe qualitatively very similar responses in quantitatively vastly different systems. Eqs. (10a), (12) and (13) have one feature in common - they all predict the effect of pressure on a system's temperature. The presence of such qualitatively similar relations in otherwise disparate physical systems can fundamentally be explained by the fact that pressure as a force per unit area represents a key component of kinetic energy (defined as force applied over a distance), while temperature is merely a physical manifestation of the available kinetic energy. Adding force (such as pressure) to a physical system inevitably boosts the system's total kinetic energy and raises its temperature. Figs. 4 and 7 suggest that this fundamental thermodynamic principle applies to systems ranging in complexity from a simple isothermal blackbody absorbing a homogeneous flux of electro-magnetic radiation to diverse planetary atmospheres governed by complex non-linear process interactions and cloud-radiative feedbacks. The hereto-identified cross-scale similarity among diverse pressure-temperature relationships could provide valuable new insights into the inner workings of planetary climate systems.

Nevertheless, important differences exist between Eq. (10a) and other simpler pressure-temperature relations. Thus, while Poisson's formula and the SB radiation law can mathematically be derived from 'first principles' and have been experimentally verified in a laboratory, Eq. (10a) could neither be analytically deduced from known basic physical laws nor accurately simulated in a small-scale experiment. This is because Eq. (10a) describes an emergent *macro-level* property of planetary atmospheres representing the net result of myriad process interactions and feedbacks in real climate systems that are not readily estimable by 'bottom-up' mechanistic approaches or fully reproducible in a laboratory environment.

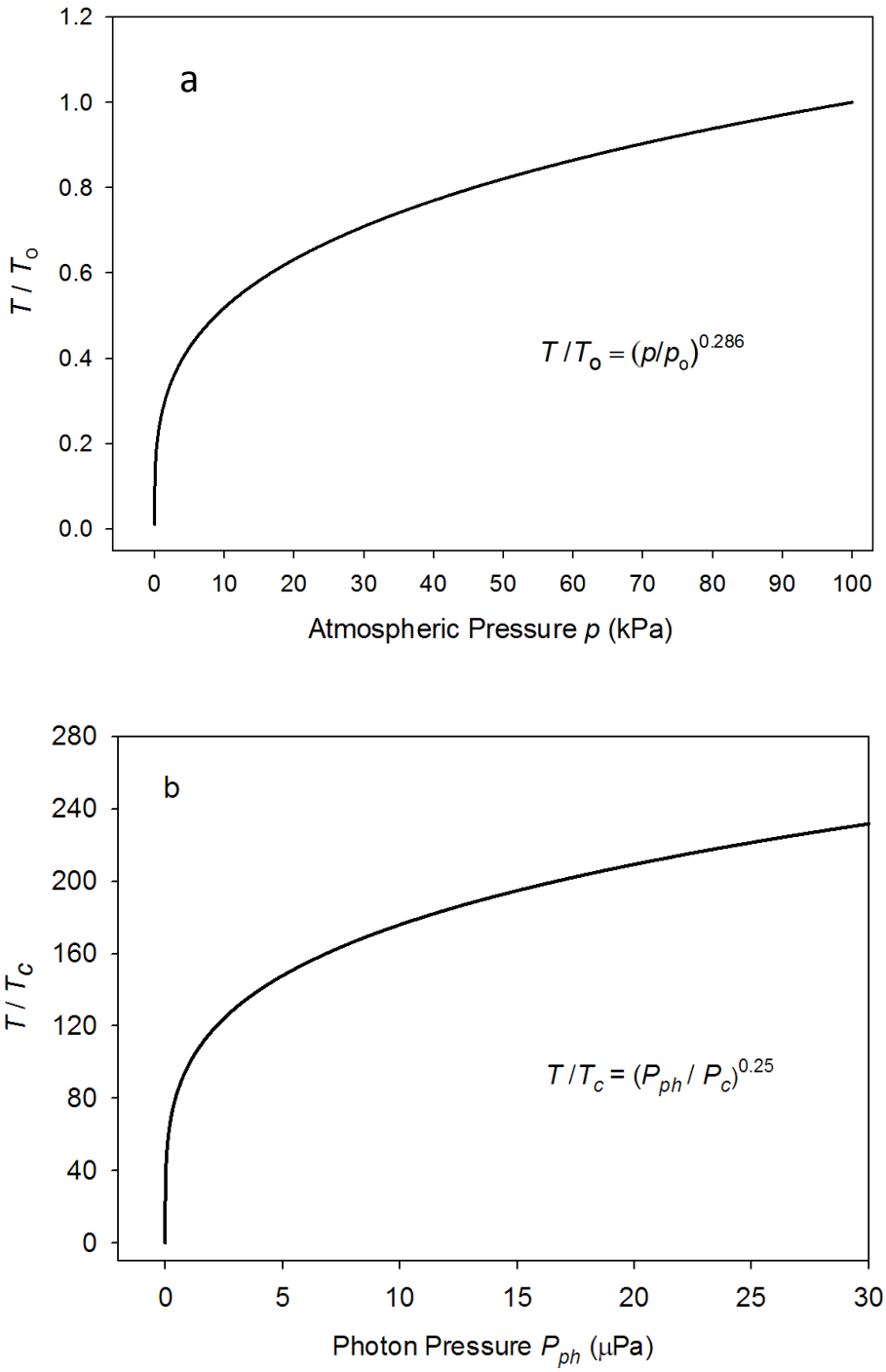

Figure 7 (*a*) Dry adiabatic response of the air/surface temperature ratio to pressure changes in the free atmosphere according to Poisson's formula (Eq. 12). The reference pressure is arbitrarily assumed to be $p_o = 100$ kPa; (*b*) The SB radiation law expressed as a response of a blackbody temperature ratio to variation in photon pressure (see text for details). Note the similarity in shape between these two curves and the one portrayed in Fig. 4 depicting Eq. (10a).

4. Model Application

Encouraged by the high predictive skill and broad scope of validity of Model 12 we decided to apply Eq. (10b) to three celestial bodies spanning the breadth of the Solar System, i.e. Mercury, Europa, and Pluto, which global surface temperatures are not currently known with certainty. Each body is the target of either ongoing or planned NASA robotic exploration missions scheduled to provide surface thermal measurements, thus offering an opportunity to test our planetary temperature model against independent observations.

The MESSENGER spacecraft launched in 2004 completed the first comprehensive mapping of Mercury in March 2013 (http://messenger.jhuapl.edu/). In addition to other observations, the spacecraft also took infrared measurements of the small planet, which should soon become available. The New Horizons spacecraft launched in January 2006 (Stern 2008) reached Pluto in July of 2015. The probe performed (among other measurements) a thermal scan of the dwarf planet during a flyby. A proposed joint Europa-Jupiter System Mission by NASA and the European Space Agency is planned to study the Jovian moons after 2020. The mission envisions exploring Europa's physical and thermal environments both remotely through a NASA Orbiter and in situ via a Europa Lander (Pappalardo et al. 2013).

All three celestial bodies have somewhat eccentric solar orbits. However, while Mercury's orbital period is only 88 Earth days, Europa and Pluto circumnavigate the Sun once every 11.9 and 248 Earth years, respectively. Hence, using Mercury's average distance to the Sun might suffice to adequately assess its mean annual surface temperature. Europa and Pluto, on the other hand, must be evaluated at least at three points along their long orbital paths, i.e. aphelion, perihelion, and the semi-major axis. The atmospheric pressure on Pluto is believed to vary over the course of its orbital period as a function of insolation-driven sublimation of nitrogen ice on the surface (Olkin et al. 2013).

Table 6 lists the average global surface temperatures of the three celestial bodies predicted by Eq. (10b) along with employed input data on orbital distances and mean surface atmospheric pressures gathered from the literature. According to our model, Mercury is 123 K cooler than NASA's current estimate of 440 K based on Eq. (3) (Williams 2013). Europa may be somewhat warmer than predicted by Eq. (10b) due to a possible tidal heating by Jupiter's strong gravitational field, which is not considered in our calculations. Our estimate of Pluto's average surface temperature at perihelion (39.3 K) is similar to the mean temperature computed for that planet by Olkin et al. (2013) using a mechanistic model of nitrogen ice volatilization at the surface. When the New Horizons spacecraft reached Pluto in July 2015, the dwarf planet was approximately 32.9 AU from the Sun and, according to our model, should have an average surface temperature between 37.3 K and 37.6 K assuming an atmospheric pressure of 4.0 Pa.

Table 6. Global average surface temperatures predicted by Eq. (10b) for Mercury, Europa and Pluto. Input data on orbital distances (AU) and total atmospheric pressure (Pa) were obtained from the NASA Solar System Exploration (2014) website, the NASA Planetary Factsheet (Williams 2014) and Olkin et al. (2013). Solar irradiances required by Eq. (10b) were calculated from reported orbital distances as described in Section 2.3.

	Surface Atmospheric Pressure (Pa)	**Modeled Average Global Surface Temperature (K) at Certain Distance from the Sun (AU) and Total Atmospheric Pressure (Pa)**		
		Aphelion	**Semi-major Axis**	**Perihelion**
Mercury	10^{-10}	-	317.4 K (0.387 AU)	-
Europa	10^{-7}	84.8 K (5.455 AU)	86. 9 K (5.203 AU)	89.1 K (4.951 AU)
Pluto	1.0 – 4.2	30.0 K (49.310 AU; 1.0 Pa)	33.8 K (39.482 AU; 2.4 Pa)	39.3 K (29.667 AU; 4.2 Pa)

One must use caution when comparing results from Eq. (10b) to remotely sensed 'average temperatures' commonly reported for celestial bodies with tenuous atmospheres such as the moons of Jupiter or Neptune. Studies oftentimes quote so-called 'brightness temperatures' retrieved at specific wavelengths that have not been subjected to a proper spherical integration. As discussed by Volokin and ReLlez (2014), due to Hölder's inequality between integrals, calculated brightness temperatures (or effective radiating temperatures) of spherical objects can be significantly higher than actual mean physical temperatures at the surface. Since Eq. (10) yields spherically averaged temperatures, it is expected to produce much lower values than the disk-integrated brightness temperatures typically quoted in the literature. For example, Moore et al. (2004) reported a disk-averaged brightness temperature of 158 K at 20 μm radiance for Jupiter's moon Callisto. Earlier, Carlson (1999) calculated a similar surface temperature (150 ± 50 K) for that moon using a theoretical model aimed at explaining an observed airglow in the carbon dioxide ν_3 band up to 100 km aboveground.

These estimates are based on 1-D models known to be prone to aggregation errors (Leconte et al. 2013; Volokin and ReLlez 2014). The physical implausibility of such disk-integrated values to represent Callisto's actual mean surface temperature can be demonstrated with the following comparison. Callisto's average distance to the Sun is 5.203 AU (NASA Solar System Exploration 2014) corresponding to a TOA solar irradiance S = 50.27 W m^{-2}. Employing this S value in the effective radiating temperature formula (Eq. 3) while assuming a Bond albedo of 0.11 (Moore et al. 2004) and a surface thermal emissivity of 0.98 produces T_e = 119.1K for that moon. This estimate is about 35 K lower than reported

brightness temperatures for Callisto. Even if one unrealistically assumes zero albedo for Callisto to maximize the effective radiating temperature, Eq. (3) still yields T_e = 122.6 K, which is ~31K cooler than the brightness temperatures inferred from disk-integrated spectral radiances by Carlson (1999) and Moore et al. (2004). Furthermore, as demonstrated by Volokin and ReLlez (2014), Eq. (3) overestimates the actual average surface temperature of airless spherical bodies by about 37%. Hence, the available solar energy at Jupiter's orbit is simply insufficient to produce a mean surface temperature of 150 K – 158 K on Callisto absent a massive geothermal flux, which has not been detected thus far. According to our model (Eq. 10b), Callisto's GMAT should be around 87 K assuming an atmospheric pressure of 7.5×10^{-7} Pa (Carlson 1999) and R_g = 0.0.

5. Conclusions

We adopted a 'top-down' statistical approach to derive a new general model for predicting the average surface temperature of rocky planets with diverse atmospheres using a well-constrained observational dataset that covers a broad range of planetary environments in the Solar System. Dimensional Analysis was employed as an objective technique to constructing relevant state and forcing variables and to ensure a dimensional homogeneity of the final model. DA suggested 12 relationships for investigation that involve dimensionless products consisting of solar irradiance, greenhouse-gas partial pressure/density and total atmospheric pressure/density as forcing variables and two temperature ratios as dependent variables. One regression model was found to statistically outperform the rest by a wide margin. Our analysis revealed that the mean annual air surface temperature of rocky planets can reliably be estimated across a broad spectrum of atmospheric conditions and radiative regimes only using two forcing variables: TOA stellar irradiance and average surface atmospheric pressure.

Based on statistical criteria including numerical accuracy, robustness, dimensional homogeneity and a broad environmental scope of validity, the final model (Eq. 10) appears to describe an emergent macro-level thermodynamic property of planetary atmospheres heretofore unbeknown to science. The potential physical significance of this new empirical relationship is further supported by its striking resemblance to the dry adiabatic temperature curve described by Poisson's formula and the photon-pressure form of the SB radiation law. Similar to these well-known kinetic relations, Eq. (10a) also predicts the effect of pressure on temperature albeit in the context of a different macro-level physical system. These characteristics of the new model call for a deeper investigation into the plausible physical mechanisms involved. For instance, the mathematical form of Eq. (10a) suggests that atmospheric pressure amplifies (through force) the energy received from the Sun creating a thermal enhancement responsible for keeping the Earth surface 90.4 K warmer than it would be in the absence of an atmosphere. In other words, Model 12 fully explains the new ~90 K estimate of Earth's total atmospheric thermal effect deduced by Volokin and ReLlez (2014) using a different line of reasoning. Eq. (10) also reveals that Earth's global temperature is a

part of a cosmic thermodynamic continuum controlled by surface air pressure (a function of total atmospheric mass) and planet's distance to the Sun.

Regardless of whether or not Eq. (10a) has any physical significance beyond a tight empirical fit, its statistical properties makes it immediately useful to planetary and astrobiological studies seeking a quick and reliable assessment of the prevailing thermal conditions at the surface of distant planets.

Appendix A. Construction of the Dimensionless π Variables

Table 1 lists 6 generic variables (T_s, T_r, S, P_x, P_r and ρ_x) composed of 4 fundamental dimensions: *mass* [M], *length* [L], *time* [T], and *absolute temperature* [Θ]. According to the Buckingham Pi theorem, this implies the existence of two dimensionless π_i products per set. We derived the π_i variables employing the following objective approach. First, we hypothesized that a planet's GMAT (T_s) is some function of all 5 independent variables listed in Table 1, i.e.

$$T_s = f(T_r, S, P_x, P_r, \rho_x) \qquad \text{(A1)}$$

This unknown function is described to a first approximation as a simple product of the driving variables raised to various powers, i.e.

$$T_s \approx T_r^a \, S^b \, P_x^c \, P_r^d \, \rho_x^e \qquad \text{(A2)}$$

where a, b, c, d and e are rational numbers. In order to determine the power coefficients we cast Eq. (A2) in terms of physical dimensions of the participating variables, i.e.

$$[\Theta] \approx [\Theta]^a \, [\mathrm{M\,T^{-3}}]^b \, [\mathrm{M\,L^{-1}\,T^{-2}}]^c \, [\mathrm{M\,L^{-1}\,T^{-2}}]^d \, [\mathrm{M\,L^{-3}}]^e \qquad \text{(A3)}$$

Satisfying the requirement for dimensional homogeneity of Eq. (A2) implies that the sum of powers of *each* fundamental dimension must be equal on both sides of Eq. (A3). This allows us to write four simultaneous equations (one per fundamental dimension) containing five unknowns, i.e.

$$\begin{cases} a = 1 & : [\Theta] \\ b + c + d + e = 0 & : [\mathrm{M}] \\ -c - d - 3e = 0 & : [\mathrm{L}] \\ -3b - 2c - 2d = 0 & : [\mathrm{T}] \end{cases} \qquad \text{(A4)}$$

System (A4) is underdetermined and has the following solution: $a = 1$, $b = 2e$, and $c = -(3e + d)$. In the DA methodology, one oftentimes arrives at underdetermined systems of equations, simply because the number of independent variables usually exceeds the number of fundamental physical dimensions comprising such variables. However, this has no adverse impact on the derivation of the sought dimensionless π_i products.

Substituting the above roots in Eq. (A2) reduces the original five unknown powers to two: *d* and *e*, i.e.

$$T_s \approx T_r^1 \; S^{2e} \; P_x^{-(3e+d)} \; P_r^d \; \rho_x^e \qquad \text{(A5a)}$$

These solution powers may now be assigned any values, although integers such as 0, 1 and -1 are preferable, for they offer the simplest solution leading to a construction of the proper π_i variables. Setting $d = 0$ and $e = -1$ reduces Eq. (A5a) to:

$$T_s \approx T_r^1 \; S^{-2} \; P_x^3 \; \rho_x^{-1} \qquad \text{(A5b)}$$

providing the first pair of dimensionless products:

$$\pi_1 = \frac{T_s}{T_r}; \quad \pi_2 = \frac{P_x^3}{\rho_x \, S^2} \qquad \text{(A6)}$$

The second pair of π_i variables emerges upon setting $d = -1$ and $e = 0$ in Eq. (A5a), i.e.

$$\pi_1 = \frac{T_s}{T_r}; \quad \pi_2 = \frac{P_x}{P_r} \qquad \text{(A7)}$$

Thus, the original function (A1) consisting of six dimensioned variables is reduced to a relationship between two dimensionless quantities, i.e. $\pi_1 = f(\pi_2)$ that needs to be investigated via a regression analysis.

Appendix B. Estimation of Mars' GMAT and Surface Atmospheric Pressure

Although Mars is the third most studied planetary body in the Solar System after Earth and the Moon, there is currently no scientific consensus regarding its mean global surface temperature (T_{M}). Reported T_{M} values span a range of 40 K. Examples of disparate GMATs quoted for the Red Planet include 200 K (Rapp 2008, p. 449), 202 K (Haberle 2013), 210 K (Williams 2013), 214 K (Taylor 2010b, p. 328), 215 K (Lacis et al. 2013; Lissauer and Pater 2013, p.115), 218 K (Vázquez and Hanslmeier 2006, p. 223), 220 K (Smil 2003, p. 107), 227 K (Schulze-Makuch et al. 2011) and 240 K (Barlow 2008, p. 163). The most frequently cited values fall between 210K and 220K. However, a close examination of the available thermal observations reveals a high improbability for any of the above estimates to represent Mars' true GMAT.

Figure B1 depicts hourly temperature series measured at 1.5 m aboveground by Viking Landers 1 and 2 (VL1 and VL2 respectively) in the late 1970s (Kemppinen et al.

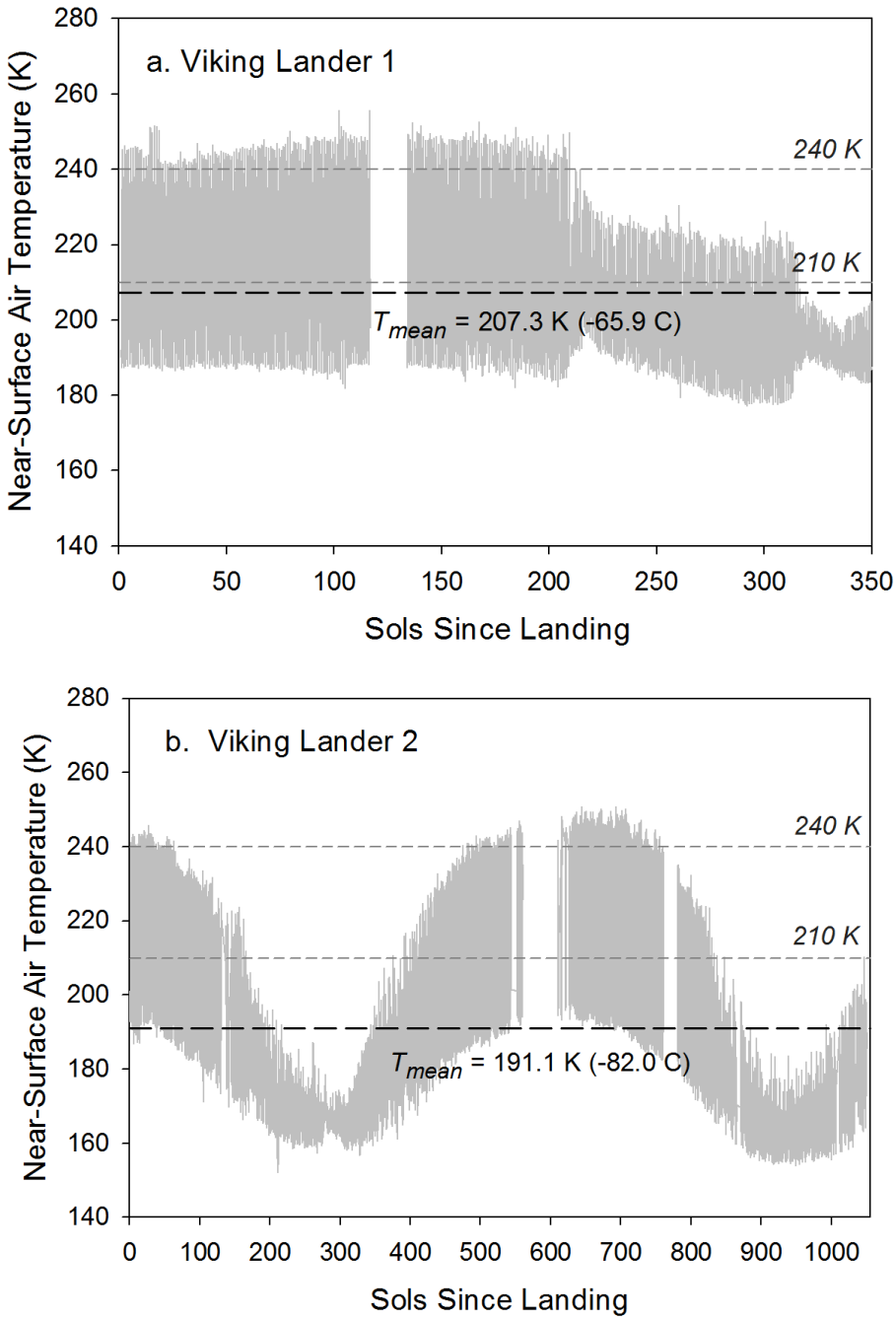

Figure B1 Near-surface hourly temperatures on Mars measured by (***a***) Viking Lander 1 at Chryse Planitia (22.48° N, 49.97° W, Elevation: -1,500 m); and (***b***) Viking Lander 2 at Utopia Planitia (47.97° N, 225.74° W, Elevation: -3,000 m) (Kemppinen et al. 2013). Black dashed lines mark the arithmetic average (T_{mean}) of each series. Pairs of horizontal grey dashed lines highlight the range of GMAT values typical reported for Mars in the scientific literature, i.e. 210 –240 K. Note that average diurnal temperatures only exceed 210 K during the summer; hence, the annual mean temperature at any Martian latitudes outside the Equator must be significantly lower than 210 K.

2013). The VL1 record covers about half of a Martian year, while the VL2 series extends to nearly 1.6 years. The VL1 temperature series captures a summer-fall season on a site located at about 1,500 m below Datum elevation in the subtropics of Mars' Northern Hemisphere (22.5^{o} N). The arithmetic average of the series is 207.3 K (Fig. B1a). Since the record lacks data from the cooler winter-spring season, this value is likely higher than the actual mean annual temperature at that location. Furthermore, observations by the Hubble telescope in mid 1990s indicated that the Red Planet has cooled since the time of the Viking mission (Savage et al. 1995; Clancy et al. 1996). Because of its thin atmosphere and the absence of significant cloud cover and perceptible water, temperature fluctuations near the surface of Mars are tightly coupled to diurnal, seasonal and latitudinal variations of incident solar radiation. This causes sites located at the same latitude and equivalent altitudes to have similar annual temperature means irrespective of their longitudes (e.g. Wilson and Richardson 2000). Hence, one could reliably estimate a latitudinal temperature average on Mars using point observations from any elevation by applying an appropriate lapse-rate correction for the average terrain altitude of said latitude.

The average elevation at 22.5^{o} latitude on Mars is close to Datum level, i.e. about 1,500 m above the VL1 site. Adjusting the observed 207.3 K temperature average at VL1 to Datum elevation using a typical near-surface Martian lapse rate of -4.3 K km^{-1} (Barlow 2008) produces ~201 K for the average temperature in the summer-fall season at that latitude. Since the mean surface temperature of a sphere is typically lower than its subtropical temperature average, we can safely conclude based on Figure B1a that Mars' GMAT is likely below 201 K. The mean temperature at the VL2 site located at 48^{o} N latitude and 3,000 m below Datum elevation is 191.1 K (Fig. B1b). The average terrain altitude between Northern and Southern Hemisphere at 48^{o} latitude is about -1,500 m. Adjusting the VL2 annual temperature mean to -1,500 m altitude using a lapse rate of -4.3 K km^{-1} yields 184.6 K. These simple calculations suggest that Mars' GMAT is likely between 185 K and 201 K.

A close examination of the Viking record also reveals that average diurnal temperatures above 210 K can only occur on Mars during summertime and, therefore, cannot possibly represent an annual mean for any Martian latitude outside the equator. On the other hand, frequently reported values of Mars' GMAT in excess of 210 K appear to be solely based on the theoretical expectation that a planet's average surface temperature should exceed the corresponding effective radiating temperature ($T_e \approx 210$ K) computed from Eq. (3) (e.g. Barlow 2008; Lacis et al. 2013). This presumption is rooted in the *a priori* assumption that T_e represents a planet's average surface temperature in the absence of atmospheric greenhouse effect. However, as demonstrated by Volokin and ReLlez (2014), due to Hölder's inequality between integrals, the mean physical temperature of a spherical body with a missing or tenuous atmosphere is always *lower* than its effective radiating temperature computed from the globally integrated absorbed stellar flux. Volokin and ReLlez (2014) also showed that Eq. (3) yields non-physical temperatures for spheres. Indeed, based on results from a 3-D climate model Haberle (2013) concluded that Mars' mean global surface

temperature is at least 8 K cooler than the planet's effective radiating temperature (210 K) estimated from Eq. (3). Therefore, Mars' GMAT must be evaluated using actual measurements rather than theoretical considerations.

In order to obtain a reliable estimate of Mars' GMAT, we calculated mean annual temperatures for several Martian latitudes employing near-surface time series measured in-situ by the Viking landers and Curiosity Rover, and remotely by the Mars Global Surveyor (MGS) spacecraft. The Radio Science Team (RST) at Stanford University utilized radio occultation of MGS refraction data to retrieve seasonal time-series of near-surface atmospheric temperature and pressure on Mars (Hinson et al. 2004; Hinson 2006; Mars Global Surveyor Radio Science Team 2007). We utilized MGS RST data between 1999 and 2005. Calculated temperature means from in-situ measurements were adjusted to the corresponding average terrain elevations of target latitudes assuming a lapse rate of -4.3 K km^{-1} (Barlow 2008). Figure B2 portrays the estimated mean annual near-surface temperatures at five Martian latitudes (gray dots) along with their standard errors. The black curve depicts a third-order polynomial fitted through the temperature averages via regression analysis and described by the function:

$$T(L) = 202.888 - 0.781801\,L - 22.3673\,L^2 - 3.16594\,L^3 \qquad \text{(B1)}$$

where L is latitude (rad). Finally, Mars' GMAT (T_M) was calculated via integration of polynomial (B1) using the formula:

$$T_M = \int_0^{\pi/2} T(L)\cos L\, dL \qquad \text{(B2)}$$

where $0 \leq \cos L \leq 1$ is a polar-coordinate area-weighting factor. The result is $T_M = 190.56 \pm 0.7$ K (Fig. B2). This GMAT, although significantly lower than values quoted in the literature, is fully consistent with the new mean surface temperature of the Moon (197.35 K) calculated by Volokin and ReLlez (2014) using results from a validated NASA thermo-physical model (Vasavada et al. 2012). Since Mars receives ~57% less solar energy than the Moon and has a thin atmosphere that only delivers a weak greenhouse effect (e.g. Pierrehumbert 2010), it makes a physical sense that the Red Planet would be on average cooler than the Moon, i.e. $T_M < 197.3$ K. Moreover, if the mean temperature at the lunar equator (Moon's warmest latitude) is 213 K as revealed by NASA Diviner observations (Vasavada et al. 2012; Volokin and ReLlez 2014), it is unlikely that Mars' global average temperature would be equal to or greater than 213 K as assumed by many studies (e.g. Smil 2003; Vázquez and Hanslmeier 2006; Barlow 2008; Taylor 2010b; Schulze-Makuch et al. 2011; Lacis et al. 2013).

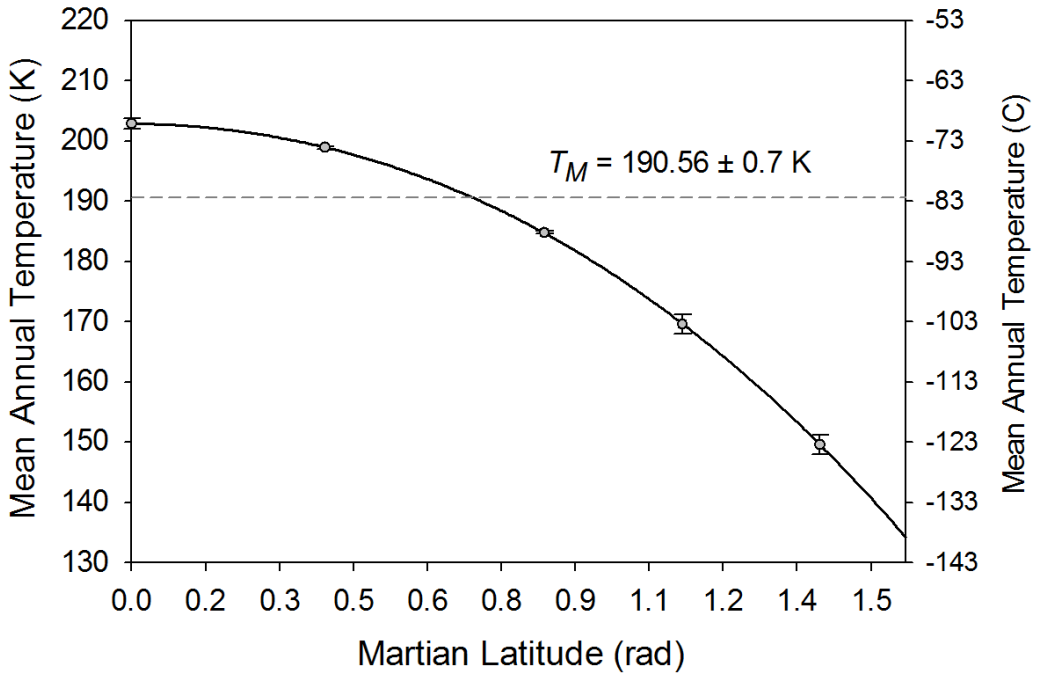

Figure B2 Mean annual surface air temperatures and their uncertainties for five Martian latitudes (gray dots) calculated from data obtained by Viking Landers, Curiosity Rover, and the Mars Global Surveyor Radio Science Team. The black curve represents a third-order polynomial (Eq. B1) fitted through the latitudinal temperature means via a non-linear regression. Mars' GMAT, T_M = 190.56 K (marked by a horizontal gray dashed line) was estimated via integration of the polynomial (B1) using formula (B2).

Published values of Mars' average surface atmospheric pressures range from 600 Pa to 700 Pa (Jakosky and Phillips 2001; Catling and Leovy 2007; Barlow 2008; Taylor 2010b; Williams 2013; Lacis et al. 2013). Since this interval was too broad for the target precision of our study, we used MGS-RST data retrieved from multiple latitudes and seasons between 1999 and 2005 to calculate a new mean surface air pressure for the Red Planet. Our analysis produced P = 685.4 ± 14.2 Pa, an estimate within the range of previously reported values.

6. References

Albertson ML, Barton JR, Simons DB (1961) Fluid Mechanics for Engineers. Prentice Hall, New Jersey.

Atreya SK, Lorenz RD, Waite JH (2009) Volatile origin and cycles: nitrogen and methane. In: Brown RH, Lebreton J-P, Waite JH (eds) Titan from Cassini-Huygens. Springer, New York, pp 177 - 200

Barlow N (2008) Mars: An Introduction to its Interior, Surface and Atmosphere. Cambridge University Press, Cambridge.

Basilevsky AT, Head JW (2003) The surface of Venus. Rep Prog Phys 66:1699–1734, doi:10.1088/0034-4885/66/10/R04

Basilevsky AT, McGill GE (2007) Surface evolution of Venus. In: Esposito LW, Stofan ER, Cravens TE (eds) Exploring Venus as a Terrestrial Planet (Geophysical Monograph Series), Wiley, 176:23-43, doi:10.1029/176GM04

Beckenbach EF, Bellman R (1983) Inequalities. Springer Verlag, Berlin.

Bender EA, (1978) An introduction to mathematical modeling. John Wiley and Sons, NY.

Bengtsson L, Bonnet R-M, Grinspoon D, Koumoutsaris S, Lebonnois S, Titov D (2013) Towards Understanding the Climate of Venus: Applications of Terrestrial Models to Our Sister Planet, ISSI Scientific Report Series, Springer.

Blanco VM, McCuskey SW (1961) Basic Physics of the Solar System. Addison-Wesley, Reading MA.

Buckingham E (1914) On physically similar systems: illustrations of the use of dimensional equations. Physical Review 4:345-376

Carlson RW (1999) A tenuous carbon dioxide atmosphere on Jupiter's moon Callisto. Science 283(5403):820-821, doi:10.1126/science.283.5403.820

Catling DC, Leovy C (2007) Mars atmosphere: History and surface interactions. In: McFadden L-A, Weissman P, Johnson T (eds) Encyclopedia of the Solar System. Academic Press, pp 301-314

Cengel YA, Turner RH (2004) Fundamentals of thermal-fluid sciences. McGraw-Hill, Boston.

Clancy RT, Grossman AW, Wolff MJ, James PB, Rudy DJ, Billawala YN, Sandor BJ, Lee SW, Muhleman DO (1996) Water vapor saturation at low altitudes around Mars aphelion: a key to Mars climate? Icarus 122 (1):36–62, doi:10.1006/icar.1996.0108

Cottini V, Nixona CA, Jennings DE, de Kok R, Teanby NA, Irwin PGJ, Flasar FM (2012) Spatial and temporal variations in Titan's surface temperatures from Cassini CIRS observations. Planetary and Space Sci., 60(1):62–71, doi:10.1016/j.pss.2011.03.015

Elliot JL, Hammel HB, Wasserman LH, Franz OG, McDonald SW, Person MJ, Olkin CB, Dunham EW, Spencer JR, Stansberry JA, Buie MW, Pasachoff JM, Babcock BA, McConnochie TH (1998) Global warming on Triton. Nature 393:765-767. doi:10.1038/31651

Fegley B, Zolotov MY, Lodders K (1997) The oxidation state of the lower atmosphere and surface of Venus. Icarus 125:416-439, doi:10.1006/icar.1996.5628

Fixsen DJ (2009) The temperature of the cosmic microwave background. ApJ 707:916, doi:10.1088/0004-637X/707/2/916

Fulchignoni M, Ferri F, Angrilli F, Ball4 AJ, Bar-Nun A, Barucci1 MA, Bettanini C, Bianchini G, Borucki W, Colombatti G, Coradini M, Coustenis A, Debei S, Falkner P, Fanti G, Flamini E, Gaborit V, Grard R, Hamelin M, Harri AM, Hathi B, Jernej I, Leese MR, Lehto A, Lion Stoppato PF, López-Moreno JJ, Mäkinen T, McDonnell JA, McKay CP, Molina-Cuberos G, Neubauer FM, Pirronello V, Rodrigo R, Saggin B, Schwingenschuh K, Seiff A, Simões F, Svedhem H, Tokano1 T, Towner MC, Trautner R, Withers P, Zarnecki JC (2005) In situ measurements of the physical characteristics of Titan's environment. Nature 438:785-791, doi:10.1038/nature04314

Griffith CA (2009) Storms, polar deposits and the methane cycle in Titan's atmosphere. Phil. Trans. R. Soc. A 367:713–728, doi:10.1098/rsta.2008.0245

Griffith CA (2007) Titan's lower atmosphere. AIP Conf. Proc. 930.1:3-36, doi:10.1063/1.2790334

Haberle RM (2013) Estimating the power of Mars' greenhouse effect. Icarus 223(1):619-620, doi:10.1016/j.icarus.2012.12.022.

Hanel RA, Pearl JC, Samuelson RE (1985) The bolometric Bond albedo of Titan. Bulletin of the Astronomical Society 17(3):739.

Hansen J, Johnson D, Lacis A, Lebedeff S, Lee P, Rind D, Russel G (1981) Climate impact of increasing atmospheric carbon dioxide. Science 213(4511):957-966.

Hansen J, Sato M, Russell G, Kharecha P (2013) Climate sensitivity, sea level and atmospheric carbon dioxide. Phil. Trans. R. Soc. A 371:20120294, doi:10.1098/rsta.2012.0294

Hayes A, Aharonson O, Callahan P, Elachi C, Gim Y, Kirk R, Lewis K, Lopes R, Lorenz R, Lunine J, Mitchell K, Mitri G, Stofan ES (2008) Hydrocarbon lakes on Titan: Distribution and interaction with a porous regolith. Geophys Res Let 35:L09204, doi:10.1029/2008GL033409

Hinson DP, (2006) Radio occultation measurements of transient eddies in the northern hemisphere of Mars. J Geophys Res 111:E05002, doi:10.1029/2005JE002612

Hinson DP, Smith MD, Conrath BJ (2004) Comparison of atmospheric temperatures obtained through infrared sounding and radio occultation by Mars Global Surveyor. J Geophys Res 109:E12002, doi:10.1029/2004JE002344

Huntley HE (1967) Dimensional Analysis. Dover Publications, New York.

Iess L, Jacobson RA, Ducci M, Stevenson DJ, Lunine JI, Armstrong JW, Asmar SW, Racioppa P, Rappaport NJ, Tortora P (2012) The tides of Titan. Science 337(6093):457-459, doi: 10.1126/science.1219631

Jakosky BM, Phillips RJ (2001) Mars' volatile and climate history. Nature 412:237-244, doi:10.1038/35084184

Jennings DE, Flasar FM, Kunde VG, Samuelson RE, Pearl JC, Nixon CA, Carlson RC, Mamoutkine AA, Brasunas JC, Guandique E, Achterberg RK, Bjoraker GL, Romani PN, Segura ME, Albright SA, Elliott MH, Tingley JS, Calcutt S, Coustenis A, Courtin R (2009) Titan's surface brightness temperatures. Astrophys J 691:L103–L105, doi:10.1088/0004-637X/691/2/L103

Jones PD, New M, Parker DE, Martin S, Rigor IG (1999) Surface air temperature and its changes over the past 150 years, Rev Geophys 37(2):173–199, doi:10.1029/1999RG900002

Kaltenegger L, Sasselov D (2011) Exploring the habitable zone for Kepler planetary candidates. Astrophys J 736:L25, doi:10.1088/2041-8205/736/2/L25

Keihm SJ (1984) Interpretation of the lunar microwave brightness temperature spectrum: easibility of orbital heat flow mapping. Icarus 60:568–589, doi:10.1016/0019-1035(84)90165-9

Kemppinen O, Tillman JE, Schmidt W, Harri A-M (2013) New analysis software for Viking Lander meteorological data. Geosci Instrum Method Data Syst 2:61–69, doi:10.5194/gi-2-61-2013

Kopp G, Lean JL (2011) A new, lower value of total solar irradiance: Evidence and climate significance. Geophys Res Lett 38:L01706, doi:10.1029/2010GL045777

Lacis AA, Hansen JE, Russell GL, Oinas V, Jonas J (2013) The role of long-lived greenhouse gases as principal LW control knob that governs the global surface temperature for past and future climate change. Tellus B 65:19734, doi:10.3402/tellusb.v65i0.19734

Lellouch E, de Bergh C, Sicardy B, Ferron S, Käufl H-U (2010) Detection of CO in Triton's atmosphere and the nature of surface-atmosphere interactions. Astron Astrophys 512, L8, doi:10.1051/0004-6361/201014339

Leconte J, Forget F, Charnay B, Wordsworth R, Selsis F, Millour E, Spiga A (2013) 3D climate modeling of close-in land planets: circulation patterns, climate moist bistability, and habitability. Astron Astrophys 554, A69, doi:10.1051/0004-6361/201321042

Li L, Nixon CA, Achterberg RK, Smith MA, Gorius NJP, Jiang X, Conrath BJ, Gierasch PJ, Simon-Miller AA, Flasar FM, Baines KH, Ingersoll AP, West RA, Vasavada AR, Ewald SP (2011) The global energy balance of Titan. Geophys Res Lett 38, L23201, doi:10.1029/2011GL050053

Lissauer JJ, Pater I (2013) Fundamental Planetary Science: Physics, Chemistry and Habitability. Cambridge University Press, New York NY.

Lucey, P Korotev RL, Gillis JJ, Taylor LA, Lawrence D, Campbell BA, Elphic R, Feldman B, Hood LL, Hunten D, Mendillo M, Noble S, Papike JJ, Reedy RC, Lawson S, Prettyman T, Gasnault O, Maurice S (2006) Understanding the lunar surface and space-Moon interactions. Reviews in Mineralogy and Geochemistry 60 (1):83–219, doi:10.2138/rmg.2006.60.2

Mallama A, Wang D, Howard RA (2006) Venus phase function and forward scattering from H_2SO_4. Icarus 182(1):10–22, doi:10.1016/j.icarus.2005.12.014

Mars Global Surveyor Radio Science Team (2007) The Daily Martian Weather Report. Online publication by Stanford University: http://nova.stanford.edu/projects/mod/.

Matthews G (2008) Celestial body irradiance determination from an underfilled satellite radiometer: application to albedo and thermal emission measurements of the Moon using CERES. Applied Optics 47(27):4981-4993, doi:10.1364/AO.47.004981

McMahon J, Scheeres D (2010) A new navigation force model for solar radiation pressure. J Guidance, Control, and Dynamics 33(5):1418-1428, doi:10.2514/1.48434

Mitri G, Showmana AP, Lunine JI, Lorenz R (2007) Hydrocarbon lakes on Titan. Icarus 186(2):385–394, doi:10.1016/j.icarus.2006.09.004

Möller F (1964) Optics of the lower atmosphere. Appl Optics 3:157-166, doi:10.1364/AO.3.000157

Moore JM, Chapman CR, Bierhaus EB, Greeley R, Chuang FC, Klemaszewski J, Clark RN, Dalton JB, Hibbitts CH, Schenk PM, Spencer JR, Wagner R (2004) Callisto. In: Bagenal F, Dowling TE, McKinnon WB (eds) Jupiter: The planet, Satellites and Magnetosphere. Cambridge University Press, pp 397-426

Morice CP, Kennedy JJ, Rayner NA, Jones PD (2012) Quantifying uncertainties in global and regional temperature change using an ensemble of observational estimates: The HadCRUT4 data set. J Geophys Res 117:D08101, doi:10.1029/2011JD017187

NASA JPL Ephemeris (2014) Horizons Web Interface: http://ssd.jpl.nasa.gov/horizons.cgi, California Institute of Technology.

NASA JPL Voyager Mission (2013) Titan. Online publication by the California Institute of Technology: http://voyager.jpl.nasa.gov/science/saturn_titan.html

NASA Solar System Exploration (2014) Planets. Online publication: http://solarsystem.nasa.gov/planets/

Neff JS, Ellis TA, Apt J, Bergstralh JT (1985) Bolometric albedos of Titan, Uranus, and Neptune. Icarus 62:425–432, doi:10.1016/0019-1035(85)90185-X

Nelson RM, Burattl BJ, Wallis BD, Smythe WD, Horn LJ, Lane AL, Mayo MJ, Simmons KE (1990) Spectral geometric albedo and bolometric Bond albedo of Neptune's satellite Triton from Voyager observations. Geophys Res Lett 17(10):1761–1764, doi:10.1029/GL017i010p01761

Niemann HB, Atreya SK, Bauer SJ, Carignan GR, Demick JE, Frost RL, Gautier D, Haberman JA, Harpold DN, Hunten DM, Israel G, Lunine JI, Kasprzak WT, Owen TC, Paulkovich M, Raulin F, Raaen E, Way SH (2005) The abundances of constituents of Titan's atmosphere from the GCMS instrument on the Huygens probe. Nature 438:779–784, doi:10.1038/nature04122

NOAA National Climatic Data Center (2014) Global surface temperature anomalies. Online publication by NOAA: http://www.ncdc.noaa.gov/monitoring-references/faq/anomalies.php

Olkin CB, Young LA, Borncamp D, Pickles A, Sicardy B, Assafin M, Bianco FB, Buie MW, de Oliveira DA, Gillon M, French RG, Gomes R Jr. A, Jehin E, Morales N, Opitom C, Ortiz JL, Maury A, Norbury M, Ribas FB, Smith R, Wasserman LH, Young EF, Zacharias M, Zacharias N (2013) Pluto's atmosphere does not collapse. Cornell University Library arXiv:1309.0841 [astro-ph.EP].

Paige DA, Foote MC, Greenhagen BT, Schofield JT, Calcutt S, Vasavada AR, Preston DJ, Taylor FW, Allen CC, Snook KJ, Jakosky BM, Murray C, Soderblom LA, Jau B, Loring S, Bulharowski J, Bowles NE, Thomas IR, Sullivan MT, Avis C, De Jong EM, Hartford W, McClees DJ (2010) The Lunar Reconnaissance Orbiter Diviner Lunar Radiometer Experiment. Space Sci Rev 150:125–160, doi:10.1007/s11214-009-9529-2

Pappalardo RT, Vance S, Bagenal F, Bills BG, Blaney DL, Blankenship DD, Brinckerhoff WB, Connerney JEP, Hand KP, Hoehler TM, Leisner JS, Kurth WS, McGrath MA, Mellon MT, Moore JM, Patterson GW, Prockter LM, Senske DA, Schmidt BE, Shock EL, Smith DE, Soderlund KM (2013) Science potential from a Europa lander. Astrobiology 13(8):740-773, doi:10.1089/ast.2013.1003

Peixoto JP, Oort AH (1992) Physics of Climate. Springer-Verlag, New York.

Pierrehumbert R (2011) Infrared radiation and planetary temperature. Phys Today 64:33-38, doi:10.1063/1.3541943

Pierrehumbert R (2010) Principles of Planetary Climate. Cambridge University Press, New York.

Peterson TC, Vose RS (1997) An Overview of the Global Historical Climatology Network Temperature Database. Bull Am Meteorol Soc 78:2837-2849, doi:10.1175/1520-0477(1997)078<2837:AOOTGH>2.0.CO;2

Rapp D (2008) Human Missions to Mars: Enabling Technologies for Exploring the Red Planet. Springer, Germany.

Rashevsky N (1960) Mathematical biophysics: physico-mathematical foundations of biology. Dover Publications, New York.

Raulin F (2008) Planetary science: organic lakes on Titan. Nature 454:587-589, doi:10.1038/454587a

Rubincam DP (2004) Black body temperature, orbital elements, the Milankovitch precession index, and the Seversmith psychroterms. Theor Appl Climatol 79:111–131, doi:10.1007/s00704-004-0056-5

Savage D, Jones T, Villard R (1995) Hubble monitors weather on neighboring planets. Hubble News Release Archive, March 21, 02:00 pm (EST): http://hubblesite.org/newscenter/archive/releases/solar%20system/venus/1995/16/text/.

Schmidt GA, Ruedy R, Miller RL, Lacis AA (2010) The attribution of the present-day total greenhouse effect. J Geophys Res 115, D20106, doi:10.1029/2010JD014287

Schinder PJ, Flasar FM, Marouf EA, French RG, McGhee CA, Kliore AJ, Rappaport NJ, Barbinis E, Fleischman D, Anabtaw A (2012) The structure of Titan's atmosphere from Cassini radio occultations: Occultations from the Prime and Equinox missions. Icarus 221 (2):1020–1031, doi:10.1016/j.icarus.2012.10.021

Schulze-Makuch D, Méndez A, Fairén AG, von Paris P, Turse C, Boyer G, Davila AF, António MR, Catling D, Irwin LN (2011) A two-tiered approach to assessing the habitability of exoplanets. Astrobiology 11(10):1041–1052, doi:10.1089/ast.2010.0592

Sharma P, Byrne S (2011) Comparison of Titan's north polar lakes with terrestrial analogs. Geophys Res Lett 38, L24203, doi:10.1029/2011GL049577

Smil V (2003) The Earth's Biosphere: Evolution, Dynamics, and Change. MIT Press.

Smith TM, Reynolds RW (2005) A global merged land air and sea surface temperature reconstruction based on historical observations (1880-1997). J Climate 18:2021-2036, doi:10.1175/JCLI3362.1

Smith TM, Reynolds RW, Peterson TC, Lawrimore J (2008) Improvements to NOAA's Historical Merged Land-Ocean Surface Temperature Analysis (1880-2006). J. Climate 21:2283-2296, doi:10.1175/2007JCLI2100.1

Steel RGD, Torrie J H (1960) Principles and Procedures of Statistics with Special Reference to the Biological Sciences. McGraw Hill.

Stephens GL, O'Brien D, Webster PJ, Pilewski P, Kato S, Li J-l (2015) The albedo of Earth. Rev Geophys 53, doi:10.1002/2014RG000449.

Stephens GL, Li1 J, Wild M, Clayson CA, Loeb N, Kato S, L'Ecuyer T, Stackhouse PW, Lebsock M, Andrews T (2012) An update on Earth's energy balance in light of the latest global observations. Nature Geoscience 5:691–696, doi:10.1038/ngeo1580

Stern SA (2008) The New Horizons Pluto Kuiper belt mission: An overview with historical context. Sp Sci Rev 140:3-21, doi:10.1007/s11214-007-9295-y

Stolk H, Gates K, Hanan J (2003) Discovery of emergent natural laws by hierarchical multi-agent systems. In: Liu J, Faltings B, Zongh N, Lu R, Nishida T (eds) Proceedings of the International Conference on Intelligent Agent Technology. *IEEE/WIC* International Conference on Intelligent Agent Technology, Halifax, Canada, pp 75-82

Taylor ES (1974) Dimensional Analysis for Engineers. Clarendon Press, Oxford.

Taylor FW (2010a) Planetary Atmospheres. Oxford University Press, USA.

Taylor FW (2010b) The Scientific Exploration of Mars. Cambridge University Press, Cambridge NY

Trenberth KE, Smith L (2005) The mass of the atmosphere: A constraint on global analyses. J Climate 18:864-875, doi:10.1175/JCLI-3299.1

Van Der Ha JC, Lappas VJ (2007) Long-term attitude drift of spinning spacecraft under solar radiation torques. Journal of Guidance, Control, and Dynamics 30(5):1470-1479, doi:10.2514/1.28506

Vaniman D, Reedy R, Heiken G, Olhoeft G, Mendell W (1991) The lunar environment. In: Heiken GH, Vaniman DT, French BM (eds.) Lunar Sourcebook: A User's Guide to the Moon. Cambridge University Press, Cambridge, pp 27-60

Vasavada AR, Bandfield JL, Greenhagen BT, Hayne PO, Siegler MA, Williams JP, Paige DA (2012) Lunar equatorial surface temperatures and regolith properties from the Diviner Lunar Radiometer Experiment. J Geophy Res 117, E00H18, doi:10.1029/2011JE003987

Vasavada AR, Paige DA, Wood SE (1999) Near-surface temperatures on Mercury and the Moon and the stability of polar ice deposits. Icarus 141:179–193, doi:10.1006/icar.1999.6175

Vázquez M. Hanslmeier A (2006) Ultraviolet Radiation in the Solar System. Springer, The Netherlands.

Vignaux GA (1991) Dimensional analysis in data modeling. In: Smith CR, Erickson G, Neudorfer PO (eds) Maximum Entropy and Bayesian Methods. Kluwer Academic Publishers, Seattle, pp 121-126

Vignaux GA, Jain S (1988) An approximate inventory model based on Dimensional Analysis. Asia-Pacific Journal of Operational Research 5 (2):117-123

Vignaux GA, Scott JL, (1999) Theory and methods: simplifying regression models using dimensional analysis. The Australian & New Zealand Journal of Statistics 41(1):31–42, doi:10.1111/1467-842X.00059

Volokin D, ReLlez L (2014) On the average temperature of airless spherical bodies and the magnitude of Earth's atmospheric thermal effect. SpringerPlus 3:723, doi:10.1186/2193-1801-3-723

Wallace JM, Hobbs PV (2006) Atmospheric Science: An Introductory Survey, 2nd edn. Academic Press, California.

Wild M, Folini D, Schär C, Loeb N, Dutton EG, König-Langlo G (2013) The global energy balance from a surface perspective. Clim Dyn 40:3107–3134, doi: 10.1007/s00382-012-1569-8

Williams DR (2014) NASA Planetary Factsheet. NASA online publication: http://nssdc.gsfc.nasa.gov/planetary/factsheet/.

Wilson RJ, Richardson MI (2000) The Martian atmosphere during the Viking mission: I Infrared measurements of atmospheric temperatures revisited. Icarus 145:555–579, doi:10.1006/icar.2000.6378

Yalin MS (1971) Theory of Hydraulic Models. MacMillan.

Younkin RL (1974) The albedo of Titan. Icarus 21(3):219–229, doi: 10.1016/0019-1035(74)90036-0

Zwillinger D (1995) Standard Mathematical Tables and Formulae. Chapman & Hall/CRC